

OSNABRÜCK UNIVERSITY

MASTER THESIS

**Optical Flow, Helmholtz Decomposition and
Autoencoders for the Characterization of Slow Waves**

A new approach for temporospatial pattern detection in neuroimaging

Author:

Michael GERSTENBERGER

Supervisors:

Dr. Dominik Jüstel

Prof. Peter König

*A thesis submitted in fulfillment of the requirements
for the degree of Master of Science*

in the

Neurobiopsychology Group
Institute for Cognitive Science

In cooperation with IBMI and ICI at Helmholtz Zentrum Munich

February 4, 2021

Declaration of Authorship

I, Michael GERSTENBERGER, declare that this thesis titled, "Optical Flow, Helmholtz Decomposition and Autoencoders for the Characterization of Slow Waves" and the work presented in it are my own. I confirm that:

- This work was done wholly or mainly while in candidature for a research degree at this University.
- Where any part of this thesis has previously been submitted for a degree or any other qualification at this University or any other institution, this has been clearly stated.
- Where I have consulted the published work of others, this is always clearly attributed.
- Where I have quoted from the work of others, the source is always given. With the exception of such quotations, this thesis is entirely my own work.
- I have acknowledged all main sources of help.
- Where the thesis is based on work done by myself jointly with others, I have made clear exactly what was done by others and what I have contributed myself.

Signed:

Date:

Abstract

Optical Flow, Helmholtz Decomposition and Autoencoders for the Characterization of Slow Waves

Neural signal transduction at different levels of alertness occurs in distinct shapes (Eger, 1981). One may observe stimulus dependent activity during wakefulness but also spontaneous patterns of activation that dominate in stages of deep sleep (Brown et al., 2012). Similarly, fast neuronal firing is replaced by slow, traveling waves of activation during anaesthesia (Steriade, Nunez, and Amzica, 1993; Celotto et al., 2020). Cortical slow waves can be captured by fluorescence microscopy of GCamp channel activity in transgenic mice at up to 100Hz.

Different types of slow waves exist which can incorporate rather localized or more widespread regions of cortex (Bernardi et al., 2018). Neocortical slow waves are distinguished from delta waves (Steriade, Nunez, and Amzica, 1993). In principle, they are thought to occur spontaneously in various regions, however it was also noted that synchrony with somatosensory states and more importantly signals in subcortical structures exists (Stroh et al., 2013). Neocortico-hippocampal synchrony is related to memory formation (Maingret et al., 2016). Recently important differences between cortical sleep slow waves and their counterpart during anaesthesia were identified (Nghiem et al., 2018). This shows that slow waves represent an important yet highly variable neural phenomenon and indicates that methods are required that allow to systematically distinguish slow waves based on their properties.

Townsend and Gong (Townsend and Gong, 2018) suggest to characterize temporospatial properties of neural recordings by the detection of patterns in Dense Optical Flow. It shows, however, that the use is accompanied by two challenges: First it shows that focal brightness changes result in sources and sinks in the vector fields. Second successful estimation of Optical Flow is challenged by the quality of the contrast it is applied on. Here it is demonstrated how both can be addressed and Dense Optical Flow used successfully to characterize slow waves. The presented procedure allows for a scale independent split of optogenetic recordings into several segments that include neocortical slow waves. This allows for an event related analysis and the computation of a contrast that is independent from anatomical structures and meets the smoothness requirements of Dense Optical Flow. It is further demonstrated that Helmholtz-Decomposition can be used to distinguish between the effect of local sources of neural activation and global patterns of neural flow. Finally, it is shown how the measured high-level features can be analysed using variational autoencoders. The approach reveals a complex topology of the distribution of different features in latent slow-wave-space. These features include the direction of flow and the distribution of sources, duration and amplitude. It shows that the combination of different types of events differs between stages of anaesthesia.

In summary a new technique to characterize slow-waves is presented that can help to improve our understanding of neural processing in the brain under anaesthesia. The use of Optical Flow, Helmholtz-Decomposition and autoencoders to characterize and distinguish different types of slow waves appears promising. It bears potentials to study the relationship between distributions of events and other features including anaesthetics, experimental stimuli or animal behavior.

Acknowledgements

I would like to thank my supervisors for their support of my Master Thesis. Especially I want to thank Silviu Bodea who initiated the project, recorded all the data and made my contribution possible. Special thanks go to him and Prof. Gil Westermeyer of the Institute of Biological and Medical Imaging (IBMI) for the continuous feedback and advice regarding the results and further direction of my work. Besides I want to genuinely thank my first supervisor, Dr. Dominik Juestel for his input regarding the methodological questions and especially for pointing out the benefits of Helmholtz-Decomposition. I truly enjoyed taking part in the meetings of his group at the Institute for Computational Biology (ICI) and appreciate that I gained interesting insights in the work of the other members which gave variety to my work during the global pandemics. Finally I want to thank my second supervisor Prof. Peter König of Osnabrück University especially for his stuctured guidance regarding a cooperation with external partners during the Master Thesis.

Contents

Declaration of Authorship	i
Abstract	ii
Acknowledgements	iii
1 Introduction	1
2 Slow waves	4
2.1 Overview: Types, functions and modes of action	4
2.2 Effects of isoflurane	6
2.3 Mechanistic models	9
2.4 Sleep slow waves and related signals	11
2.4.1 Three systems for sleep regulation	11
2.4.2 Neural oscillators and relays for ascending activation	14
2.5 Sleep slow waves and memory consolidation	21
2.6 Neocortical slow waves: Towards a working definiton	23
3 Methods	28
3.1 A new approach to track intracerebral blood flow	28
3.2 Dense Optical Flow	33
3.3 Helmholtz Decomposition	37
3.4 Autoencoders	42
3.5 The processing pipeline	49
4 Results	53
4.1 Qualitative and quantitative descriptions of slow waves	53
4.2 Reconstruction manifolds and latent space distributions	60
5 Discussion	67
Bibliography	70

List of Figures

2.1	Oscillatory centres and the ascending reticular activation system	15
2.2	Frequencies of slow waves differ between measuring techniques	27
3.1	Processing pipeline for the detection of bloodflow	29
3.2	A mean shift approach for clustering pixels	30
3.3	Cluster tracking reveals trajectories of oxygenated hemoglobin	31
3.4	Levelsets and Optical Flow	34
3.5	Helmholtz decomposition of a sample vector field	39
3.6	Optical flow for a simulated signal	41
3.7	Helmholtz Decomposition of Optical Flow	42
3.8	Structure of the MLP Autoencoder	46
3.9	Structure of the mixed input Autoencoder	47
3.10	Structure of the Autoencoder for time series analysis	48
3.11	Outline of the approach	50
3.12	The processing pipeline	52
4.1	Detected slow waves for a sample recording	53
4.2	Distribution of the peak amplitude of detected waves	54
4.3	Typical examples and peak amplitudes	55
4.4	A typical example with one peak	56
4.5	Direction of flow for different levels of isoflurane	57
4.6	A sample vector field and field strength of flow in time.	58
4.7	The temporal mean of the df/f signal and the sources	58
4.8	Slow wave subsegments	59
4.9	Latent slow wave shape space	61
4.10	Examples for reconstructions of the mixed input model	62
4.11	Latent slow wave space	65
4.12	Latent slow wave flow space	66

List of Abbreviations

EEG	Electroencephalogram
ECoG	Electrocorticogram
fMRI	Functional Magnetic Resonance Imaging
MRI	Magnetic Resonance Imaging
CT	Computed tomography (X-ray)
GCaMP	A genetically modulated calcium channel with green fluorescence
K+	Potassium ions
Ca2+	Calcium ions
NMDA	N-Methyl-D-Aspartic-Acid
GABA	Gamma-Aminobutyric-Acid
iso	Isoflurane
ARAS	Ascending reticular activation system
RMT	Rostral midline thalamic nucleus
LP	Lateral posterios nucleus of thalamus
MnPO	Medial nucleus of the preoptic area
RTN	Reticular thalamic nucleus
SCN	Suprachiasmatic nucleus
VLPO	Ventrolateral nucleus of the preoptic area
MnPO	Medial nucleus of the preoptic area
RSD	Retrosplenial Dysgranular
REM	Rapid eye movement
RBF	Radial basis function
CNN	Convolutional neural network
VAE	Variational Autoencoder
UNet	Autoencoder with U-shape
MLP	Multilayer perceptron where all layers are fully connected.
RELU	Rectified linear units

Chapter 1

Introduction

Anaesthesia inhibits neural activity and alters the signals in the brain. Depending on the dosage of the anaesthetic in use different patterns can be observed (Eger, 1981). At intermediate concentrations many agents cause propagating low-frequency waves that occur in close succession and manifest as slow oscillations in EEG (Steriade, Nunez, and Amzica, 1993; Eger, 1981). Similar patterns can be observed during deep sleep. Neocortical slow waves differ in shape and size and with respect to specific temporo-spatial features: Most importantly the source location of recurrent activation, the direction and speed of spread and different sets of functionally connected regions can be observed (Brown et al., 2012). These features can be measured using modern imaging techniques that capture the fluorescence of genetically modified GCamp channels.

The development of new experimental technologies to capture GCamp fluorescence with an increasing temporal resolution of up to 100Hz offers new opportunities for the study of the neural circuitry and dynamic state changes of the brain under anaesthesia. At the same time, they also impose new challenges that result from the complexity of the recorded data. These challenges must be addressed by a well-controlled experiment or suitable approaches for data analysis.

Strict experimental control simplifies data processing. Under certain experimental conditions, high amplitude slow waves with a good signal to noise ratio and contrast to the hemodynamic autofluorescence occur in a regular pattern. For ketamine induced anaesthesia (100mg/kg), regular patterns of neocortical slow waves with highly similar shapes, durations and amplitudes occur. This simplifies the separation of events and the subsequent analysis (Celotto et al., 2020). However, such strict control means that the variance of

the captured slow waves is highly reduced.

More general findings regarding the structure of neocortial slow waves are only possible in less controlled settings. This means, however, that suitable methods for data processing and analysis must be established that are both robust and suitable to capture the dynamics of neocortical slow waves of different shapes and signal strengths.

Hence a new approach was developed that allows to distinguish and characterize neocortical slow waves of various shapes and forms. It reveals a complex topology of events and shows how different levels of isoflurane change the way signals travel in the brain. The development was accompanied by two major questions: (1) What are slow waves and (2) how can their temporospatial properties be measured and characterized. To answer the earlier question and provide a working definition for neural slow waves that allows to distinguish different events, relevant slow wave literature was systematically reviewed. To tackle the latter question, it was investigated how Dense Optical Flow can be used to measure the strengths and direction of neural flow and how Helmholtz Decomposition can help to distinguish it from neural sources and areas of extended recurrent activity. As not only features but characteristic patterns are of interest it was further assessed how autoencoders can be used for dimensionality reduction of the measured properties. In the following the results of named literature review are presented first (section 2). It shows that anaesthetics change important properties of neurons most prominently their excitability which explains why bistable states of network activity that can be observed in neocortex empirically (see section 2.2). While important differences exist between anaesthesia and sleep, slow waves can be observed in both states. One may distinguish corticothalamic slow waves in the delta range and neocortical slow waves of a duration above one second (see section 2.4). The latter kind of slow waves is of main interest here. They are understood as extended periods of recurrent neural activation that manifests as above baseline activity (see section 2.6).

The methods to analyse slow waves are explained in the second part. First a new approach is presented that allows to track haemoglobin rich blood in vessels of various size. It is shown that high amplitude oscillations result from intracranial blood flow and band-stop filtering can be used to reduce this effect. Second an overview of the processing steps is provided. The

procedure of splitting events is reported, then Dense Optical Flow is introduced, and it is demonstrated how Helmholtz Decomposition can be used to distinguish between the effect of local brightness changes and global flow. Subsequently the use of autoencoders for unsupervised characterization of slow waves is discussed and the hyperparameters of the models used are presented.

The results of the approach are shown in the third part. First simple statistics regarding the dataset, selected features and the experimental conditions are reported. Then the relationship between properties of waves is summarized for representative events. Finally, the results of the autoencoders are reported.

In the last part the findings regarding the methods and the achieved results are discussed. Optical-flow, Helmholtz decomposition and autoencoders are a suitable tool to study slow waves. Feature engineering helps to select relevant and robust features. Optical flow can be used in combination with Helmholtz-Decomposition to distinguish between local sources and global pathways of neural flow. Autoencoders represent an easy-to-use tool for the analysis of high-level features. The results confirm the existence of fundamentally different types of slow waves. The approach allows for a fine-grained distinctions and reveals a complex topology of static and dynamic properties in latent slow wave space.

Chapter 2

Slow waves

2.1 Overview: Types, functions and modes of action

There is a large body of literature that addresses slow oscillations in the brain. Slow waves in the delta range (0.5-4 Hz) can be identified in electroencephalograms (EEG) in deep sleep and under anaesthesia. Neurons that switch between up and down states in the respective frequency are present in thalamus indicating that this kind of slow waves is of thalamic origin. As they interact with cortex they are referred to as thalamocortical slow waves here (Steriade and Deschenes, 1984; Brown et al., 2012). Since their discovery by Steriade et. al (1993) a different type of slow waves, that occurs with a frequency below 1Hz has been studied extensively as well: Neocortical slow oscillations. As they do not necessarily occur in regular time intervals they are referred to as neocortical slow waves here (see also section 2.6). Both electrophysiological recordings as well as fluorescence microscopy have been used to investigate neocortical slow waves (Niethard et al., 2018; Celotto et al., 2020). Neocortical slow waves with a typical duration of more than one second are the main subject of the empirical analysis presented here.

On one side neocortical and thalamocortical slow waves are recognized as distinct phenomena (Brown et al., 2012, p. 1110). On the other side it was found that both signals relate can occur in an orchestrated way. One interpretation is that neocortical slow oscillations bind together spindles and delta waves (Brown et al., 2012, p. 1110). While named signals are of different origin one could hence consider them to be the signature of a single, yet distributed process. To better understand how distinct oscillatory patterns in the brain relate to neocortical slow waves is crucial to summarize our knowledge about them. Hence selected examples for literature on slow waves, sleep and the effect of anaesthetics are briefly discussed in this chapter. Herein the aim

is not to provide a full literature review but to present relevant information that is necessary to discern events, measure their properties and interpretate the results achieved ¹.

Anaesthesia with isoflurane has several effects on the properties and the spiking behaviour of neurons. The modes of action of anaesthetics such as isoflurane have been studied extensively (Qazzaz and Winlow, 2017; Moghadam et al., 2019; Eger, 1981; Jenkins, Franks, and Lieb, 1999). Although the precise mechanisms are not fully understood it shows that anaesthetics change several properties of neurons and reduce their excitability which explains widespread quiescence at deep levels of anaesthesia. At intermediate levels bistable states can be observed in which slow waves of distinct shapes occur (see section 2.2).

The question how bistable states arise from the interaction of cells in neural networks has been addressed using spiking network models. They provide an explanation for the occurrence of neocortical slow waves during deep sleep and under anaesthesia. The circumstance that several models exist highlights not only that different explanations are possible but also that different kinds of processes might exist (Nghiem et al., 2018). Bistable states occur both during sleep and during anaesthesia. However important characteristics of the dynamics of neocortical slow waves differ between these states. Hence it was argued that two different types of slow waves occur during sleep and anaesthesia (see section 2.3).

Evidence from several decades of research highlights the role that thalamic circuits play for the generation of rhythmical activity, the awake state and slow wave sleep (Brown et al., 2012). In contrast to anaesthesia sleep is a vegetative state. The decrease in excitation that can be explained by the interaction of anaesthetics and membrane proteins is arguably achieved by processes that include the suppression of excitatory signals from the ascending reticular activation system (ARAS) during deep sleep. Thalamic nuclei play a crucial role in the generation of neural oscillations including spindles and slow waves in the delta range. While slow wave sleep is arguably promoted by several mechanisms including the circadian cycle and the release of melatonin that alters neural excitability, sleep spindles of thalamic origin are assumed to be the trigger for a transition to deep sleep (Montagna, 2005, p. 347). Besides, specific regions have been identified in thalamus that oscillate

¹For a complete review on neocortical slow waves see (Neske, 2016).

in the delta range (Steriade and Deschenes, 1984). Sleep spindles also precede many of the neocortical slow waves that were observed on the level of single cells using two-photon imaging (Niethard et al., 2018). This contrasts with the assumption that neocortical slow waves form in a spontaneous and fully independent manner in neocortex if the excitability is reduced (see section 2.4).

A putative function of neocortical slow waves is memory consolidation. The assumed modes of action have been described in the hippocampo-neocortical dialog model (Buzsáki, 1996). Many results support the hypothesis that memory replay occurs during sleep and that it includes both hippocampus and neocortex. One may hypothesize that neocortical slow waves represent the neural signature of an important part of this process. Memory consolidation is arguably the most prominent cognitive function of slow waves (see section 2.5).

As explained above slow waves differ with respect to several features. This holds both for the duration and frequency at which they occur and the assumed sites of origin. Neocortical slow waves can emerge from various regions. EEG studies in humans indicate that prefrontal-orbitofrontal regions act as the preferred source location (Brown et al., 2012, p. 1110). First steps to distinguish slow waves in a data driven approach were carried out by Bernardi et al. (2018). Two types of sleep slow waves may be distinguished in EEG. This distinction is based on a metric that includes a shape parameter and a term that indicates whether slow waves are rather local or widespread. The distribution of these types of slow waves differs during different stages of deep sleep. It highlights the importance of means to discern slow waves based on their shape and spatial patterns of activation. A working definition that allows to detect and separate slow waves is derived from the developed understanding of slow waves (see section 2.6).

2.2 Effects of isoflurane

Anaesthetics alter the spiking behaviour of cortical neurons. Under deep anaesthesia the activity of cells is highly reduced, and quiescence can be observed for most units. However, the modes of action that cause the respective changes of neural properties differ between anaesthetic agents. In addition, the effects can depend on the exact concentration of the drug in use and low

dosages may, in some cases, even have opposing effects (Moghadam et al., 2019). As isoflurane was used during dataset acquisition its effects on the cell membrane are shortly summarized while important differences to other anaesthetics are highlighted whenever necessary. It is known that alterations of the properties of individual cells change the dynamics of neural interaction on a population level. By adjusting the properties of cells in simple models of neural networks bistable states can be reproduced that resemble slow waves under anaesthesia (Jercog et al., 2017).

The exact pharmacological mechanisms of action of inhalant anaesthetics such as isoflurane remain uncertain (Miller, Theodore, and Widrich, 2020). Effects on several ion channels have been reported including both chemically gated CL- channels (GABA receptors and glycine receptors) and K+ channels (Glutamate receptors). For example, isoflurane is known to reduce the hyper potentiation that results from CL- influx as a consequence of in vitro GABA administration (Jenkins, Franks, and Lieb, 1999). Hence it can be assumed to have excitatory effects in the nervous system as it decreases the inhibition due to GABA. However, isoflurane also has inhibitory effects as it suppresses K+ channel currents resulting in smaller electrically triggered peak amplitudes of action potentials (Buljubasic et al., 1992). Besides a potentiation of glycine receptors is assumed alongside other neurochemical mechanisms that alter the excitability of neurons (Biotechnology Information, 2021). In vivo studies indicate that the net-effect of isoflurane is inhibitory for all relevant dosages. In this respect isoflurane contrasts with other anaesthetics (including e.g. halothane and ketamine) that show concentration dependence (Moghadam et al., 2019). It shall be noted however that differences in the density of different types of receptors exist in different areas of the brain. While isoflurane can be assumed to decrease the excitability of neurons and inhibit neural signalling at all concentrations this effect could differ between brain areas.

Single cell recordings reveal decisive effects of isoflurane on the properties and the spontaneous behaviour of neurons. Moghadam et. al (2019) performed a comparative study of systemic and volatile general anaesthetics in single cell cultures and the isolated brain of lymnaea stagnalis. The substances tested include the volatile agents sodium pentobarbital, sodium thiopentone, ketamine on one side as well as halothane, enflurane and isoflurane on

the other. It was found that isoflurane causes a gradual decline of both amplitude and frequency of spontaneous action potentials. Differences between the six types of neurons studied were found to be marginal. Upon stimulation neurons remained silent at all examined concentrations of isoflurane. In contrast a gradual decline of evoked action potentials showed for increasing levels of enflurane. Using either halothane or barbiturates the authors were also able to produce bistable states *in vitro* during which periods of rapid spiking and quiescence alternate spontaneously (Moghadam et al., 2019).

Besides named alternations in spiking, effects on subthreshold properties of neurons have been identified. Increasing levels of isoflurane can cause a decrease in the membrane time constant i.e. the duration between stimulus onset and 63% potential change of the cell membrane. Under normal conditions it takes longer for the neuron to reach maximal voltage as compared to anaesthesia with isoflurane. This is reflected in the estimated membrane capacitance that analogously decreases. The membrane capacitance is especially interesting because of the role it plays in the integration of electrical inputs (Golowasch and Nadim, 2014). The most likely explanation for the apparent reduction is an increase in the leakage current. This is because it is (1) rather unfeasible for the capacitance of the membrane to alter significantly as its surface area does not change and (2) because of the abovementioned interaction between membrane proteins and anaesthetics (Qazzaz and Winlow, 2017). Neurons act as temporal integrators and fire if the combined voltage of input spikes that occur simultaneously or in short succession exceeds the threshold. If the leakage current is stronger the timing of input spikes becomes more critical as the membrane potential goes back to baseline more quickly which may prohibit charge accumulation. Hence it can be hypothesized that anaesthetics could affect the temporal integration of signals.²

While named effects explain the inhibition of neural firing under anaesthesia for different amounts of isoflurane decisive effects arise on the population level. Eger (1981) systematically studied the EEG patterns in the awake state and during anaesthesia with isoflurane for five different dosages at up to 2.9% in humans. For very light anaesthesia ($\text{iso} = .56\%$) low voltage fast activity can be observed. At a light surgical level ($\text{iso} = .96\%$ and 1.78%) slow oscillations are present that change from more regular to irregular patterns

²Note that other anaesthetics were found to increase the membrane capacitance

and alternating patterns with high amplitude oscillations at a moderate surgical level ($\text{iso} = 2.2\%$). For deep anaesthesia only occasional low voltage activity shows ($\text{iso} = 2.9\%$). Isoflurane administration leads to a gradual shift from a stable awake state to bistable states and finally deep anaesthesia where quiescence dominates.

It shows that inhalant anaesthetics interact with ion channels in the neural cell membrane. The overall effect is a reduced excitability that causes quiescence at high dosages. In contrast intermediate concentrations lead to a gradual change from a steady up state to more or less regular slow waves that occur sporadically at deep anaesthesia. Slow oscillations can be observed in the brain at intermediate levels of anaesthesia.

2.3 Mechanistic models

The effects of anaesthesia that are presented here provide the background for a mechanistic interpretation of slow wave activity. The dynamics that arise from changes of neural properties can be modelled using spiking artificial neural networks. Several networks have been proposed.

For example, features of slow waves can be produced with a simple model that employs Adaptive Exponential Integrate and Fire cells as shown by Nghiem et al. (Nghiem et al., 2018): Simulations of a network that consists of 80% excitatory cells and 20% fast spiking inhibitory neurons produce sequences of continuous activity (up states) and widespread absence of action potentials (down-states). A shift from down-states to an up state can be triggered by background noise while "spike-frequency adaptation on excitatory cells produces a self-inhibition that, destabilizing the up state, causes a reset to the down state" (Nghiem et al 2018, p. 2). Spiking network models can reproduce alternating sequences of up states and down states, an important characteristic of population level activity under anaesthesia.

A model that explains sleep slow waves on the level of ion channels is the averaged neuron model. Accordingly, a slow wave occurs because of an increase in Ca^{2+} concentration in the cell that can trigger Ca^{2+} gated K^+ channels. During the slow wave up state intracellular Ca^{2+} is assumed to activate concentration dependant K^+ channels which result in a membrane hyperpolarization due to K^+ efflux. Accordingly a hyperpolarization prohibits a

depolarization that can trigger action potentials and hence leads to the transition to a down state. "These results suggested that activity-dependent K⁺ channels, such as KCa, might be crucial for the termination of Up states" (Neske, 2016). Synaptic depression could play an additional role for the observed population level refractory period after the slow waves. The K⁺ channel conductance is hypothetically modulated by cascades of reactions that include chemical messengers during sleep (Shi, Millius, and Ueda, 2019). The transition to the bursting phase (up state) of the slow wave is assumed to be initiated by Ca²⁺ influx due to activation of NMDA receptors and voltage gated Ca²⁺ channels (Shi and Ueda, 2018). NMDA receptors are triggered by excitatory neurons that release glutamate. Layer five pyramidal neurons which represent the most abundant cell type in cortex are arguably the key players. Continuous firing during up states can be explained by recurrent activation that is moderated by interneurons (Neske, 2016). In sum the averaged neuron model states that incoming signals from glutaminergic neurons can trigger up states by activation of NMDA receptors whereas a transition to the down state is explained by accumulation of Ca²⁺ in the cells. (Shi, Millius, and Ueda, 2019).

While simple mechanistic models explain important features of slow waves during sleep and anaesthesia on a population level, they rely on the formalization of processes that are in their entirety not fully understood. It was highlighted that the exact mechanisms of action of anaesthetics remain uncertain. Generalizing over different agents and dosages is not justified in all cases and the dynamic of neural signalling might be affected by differences in the distribution of receptors for different neurotransmitters in different structures of the brain. Besides the complex anatomy of the brain including the architecture of various pathways that connect different regions uni- or bidirectionally is typically not reflected in simple mechanistic models. More precise measurements of the pathways and dynamics of neural signal transduction during slow wave anaesthesia are necessary to understand bistable states of the brain. This is especially important also because it was recently shown that slow wave sleep differs significantly from anaesthesia.

2.4 Sleep slow waves and related signals

Recently it was argued that the dynamics of slow wave sleep and slow wave anaesthesia differ substantially (Nghiem et al., 2018). Jercog et al. (2017) found that the length of up states and the subsequent down state is correlated during urethane induced anaesthesia in rats for clearly synchronized periods where high-amplitude, slow fluctuations are present in local field potentials. Coefficients indicate a very weak relationship ($r = .2$). However, the correlation was found to be consistently positive across experiments whereas the correlation with later down-state periods (time-lag > 2) is close to zero (Jercog et al., 2017). This pattern in the dynamic of neural firing can be reproduced using simple mechanistic models (see section 2.3). During human non-REM sleep, however, no such relationship holds. As a tendency, long down states are followed by short up states instead as indicated by a very weak but significant negative correlation ($r = -.04$). A negative peak in the temporal cross correlation exists around zero (Nghiem et al., 2018). This gave rise to the argument that sleep-slow waves are fundamentally different from their counterpart during anaesthesia and represent two distinct types (Nghiem et al., 2018). Hence the mechanisms that enable slow wave sleep are more closely examined in this section.

2.4.1 Three systems for sleep regulation

It is long known that the anatomical substrate of sleep is a distributed system rather than a single region in the brain(Akert, 1965). Mammalian sleep represents a physiological process that is arguably regulated by the interaction between various control mechanisms. In general, one may categorize these processes into three classes each of which affects the activity of cortical neurons directly or via intermediate events.

- (1) First there are processes that decrease neural excitability rather unpecifically by a release or an accumulation of disperse chemical messengers such as the neurohormone melatonin.
- (2) Second processes exist that incorporate electrical signalling via action potentials. They include the neurotransmitter systems that correspond

to the ascending reticular activation system (ARAS). Ascending projections from other areas (e.g. thalamic nuclei) that increase the neocortical arousal in a spatially rather unspecific manner can be subsumed under this category as well.

- (3) Third there are processes that lead to oscillations in the firing rate of distinct neural populations. The latter can include spike rates that follow the circadian rhythm and alter both the release of neurohormones and the excitation of cortex via spiking activity. However oscillatory activity also occurs in the delta range and the frequency of neocortical slow waves.

As it is not possible to discuss all features of sleep here, important examples are presented that fall under named categories. The aim is to characterize the circumstances under which sleep slow waves occur³.

Melatonin is the messenger of a system for sleep regulation that falls under the first category. In healthy subjects, melatonin concentrations alternate according to the cardiac cycle (Montagna, 2005). Melatonin can pass the blood brain barrier and can hence diffuse to the central nervous system where it accumulates (Aulinas, 2019). It acts as a neurohormone and has an inhibitory effect on cortical neurons via different modes of action. Melatonin receptors in the neural membrane have been identified. Besides it was found that melatonin interacts with voltage sensitive Ca²⁺ channel and inhibits the release of neurotransmitters as well as synaptic transmission (Choi et al., 2014). As it decreases the neural excitability of cortical neurons it shares some of the effects of mild anaesthesia. Melatonin reduces the excitability of disperse populations of neurons in the central nervous system promoting drowsiness and sleep.

The suprachiasmatic nuclei (SCN) represent an example for the third of the abovementioned categories. It interacts with the melatonin system. Melatonin is produced by pinealocytes that compose 95% of the cells in the pineal gland (Aulinas, 2019). The pineal gland resides outside the blood brain barrier and extends hypothalamus ventrally. It represents an interface between neural signalling and the endocrine system and is innervated by centres in the brain stem. Most importantly it is known to receive signals which are

³For a good review with a focus on sleep that includes a discussion about the origins of different kinds of rhythms in the brain see Brown et al. (2012).

related to retinal activity from the SCN. The SCN is capable not only of creating a light-dependant circadian rhythm, but also of maintaining an entrained rhythm (Koella, 1984). The latter could be demonstrated in electrophysiological recordings in vitro. Isolated SCN show firing rates that alternate in a 24-hour pattern (De Berardis et al., 2011). Arguably this explains changes of melatonin release that follows the circadian cycle.

While melatonin is evidently part of sleep regulation the transition between the awake state and slow wave sleep is arguably initiated by other mechanisms. Mammalian sleep can be triggered by electrical stimulation of the thalamus. First experiments were carried out using cats while later experiments confirmed that the effect exists for dogs as well (Akert, Koella, and Hess Jr, 1951; Akimoto et al., 1956). A stimulation of the intralaminar thalamus of cats with a duration of 30-60 seconds and pulses at 4-8Hz leads to a transition to sleep. This transition occurs in different stages. Sleep spindles occur while the animal is still awake. After several minutes, a full transition to slow wave sleep can be observed (Akert, Koella, and Hess Jr, 1951). These early studies indicate that thalamocortical sleep spindles play an important role for the transition to sleep.

Early lesion studies indicated that brainstem nuclei are required for both normal awake activity and rapid eye movement (REM) sleep. In animals with a Cerveau isolé preparation no normal sleep patterns can be observed. Instead one may synchronize firing that manifests in slow waves with a main frequency of around 1 Hz (Kawamura and Domino, 1968). In named preparation ascending fibers between pons and midbrain are dissected. Effectively large parts of the reticular formation and several nuclei that use specific neurotransmitters are disconnected from midbrain, thalamus, and cortex. In contrast an encéphale isolé preparation in which the brain and the spine are separated does not have named effects but normal sleep patterns can be observed. This highlights the importance of brain stem for the regulation of sleep and alertness. Named nuclei include serotonergic neurons in the raphe nucleus, norepinephrine neurons in locus coeruleus and glutamate neurons in the pedunculopontine nucleus. They represent the most important excitatory neurotransmitters. These nuclei are known as the source of the ascending reticular activation system that is known to promote alertness (Brown et al., 2012).

Similar to target sites in thalamus electrical stimulation of the raphe nuclei

induces sedation and sleep in rats (Kostowski et al., 1969). The raphe nuclei are brain stem areas that represent the origins of the ascending serotonergic pathways. Together with several neighbouring cores they provide excitatory input to large populations of cortical neurons and hence facilitate firing via different pathways. If the activity of the raphe nuclei is reduced by electrical stimulation the arousal of neocortex consequently decreases (see 2.4.2). Mechanisms that lead to a transition to sleep modulate the activity of ascending pathways of the ARAS including the serotonergic system which increase cortical activation.

It shows that the mechanisms that regulate sleep decrease the excitability and activation of cortical neurons under the contribution of chemical messengers including melatonin and an inhibition of the ascending arousal system. Subcortical nuclei can produce oscillatory patterns that reflect the circadian cycle whereas thalamus plays a key role in the transition from an awake state to deep sleep. Deep sleep represents a bistable and is characterized by a switch between up and down states of cortical activity. Thalamic nuclei are known to produce sleep spindles which are considered a switch for the transition between light and deep sleep (Montagna, 2005). Besides sleep spindles, thalamic regions generate rhythmical activity that oscillates in the delta range. Neocortical slow waves that arise during sleep arguably interact with these rhythms. The underlying processes are more closely examined in the next section.

2.4.2 Neural oscillators and relays for ascending activation

Both the transition to the bistable state of slow wave sleep and fluctuations in the delta range include ascending signals that originate from subcortical areas. Several centres have been identified that generate oscillatory patterns of spiking activity. These patterns include (1) thalamocortical sleep spindles, (2) hippocampal sharp wave ripples (3) delta waves of thalamic origin and (4) neocortical slow waves. Distinct pacemakers exist which neural oscillators and cause named rhythms in the brain.

Rostral midline thalamus: A relay for ascending activation

The circumstance that slow waves were measurable in the cerveau isolé preparation indicates that slow waves are initiated in brain regions above pons.

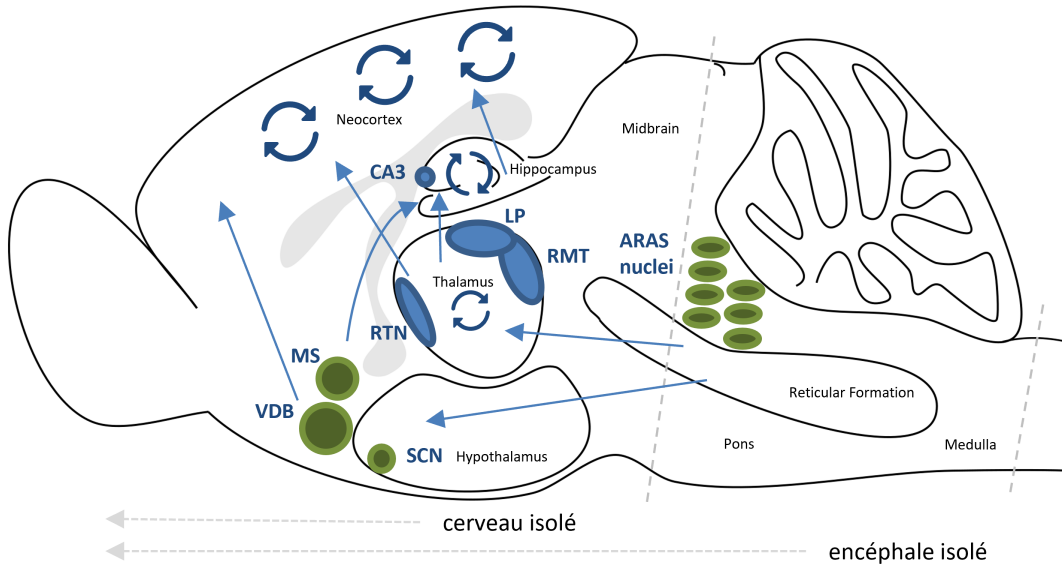


Figure 2.1: Oscillatory centres and the ascending reticular activation system. Circular arrows illustrate sites that act as neural oscillators. Thalamocortical slow waves in the delta range are assumed to originate from the lateral posterior nucleus of thalamus. Thalamocortical sleep spindles are produced in the reticular thalamic nucleus. Rostral midline thalamus (RMT) arguably acts as a relay for the ARAS and abolishes delta waves. It projects to cortex in a non-specific manner. Hippocampal sharp-wave-ripples arise in the subfield CA3 of hippocampus proper. Slow cortical oscillations ($<1\text{Hz}$) and high frequency waves arguably arise in neocortex. Straight arrows indicate the lateral and dorsal pathways of the ascending reticular activation system. Note that centres in the basal forebrain (BF) may suppress the generation of hippocampal short-wave-ripples. Arrows do not relate to the anatomical location of projection fibres and indicate no preferential sites within the target structure. The transections of the preparations “ceveau isolé” ad “encephalé isolé” are indicated by dotted lines. Slow waves occur in the cerveau isolé while normal sleep patterns have been observed for encephalé isolé. Abbreviations: Reticular thalamic nucleus (RTN), Lateral posteros nucleus (LP) Medial nucleus of the preoptic area MnPO and ventrolateral nucleus of the preoptic area (VLPO), Basal forebrain including the Medial septum (MS) and the Vertical Limb of the Diagonal Band (VDB), suprachiasmatic nucleus (SCN), rostral midline thalamus (RMT), Nuclei of the ascending reticular activation system (ARAS nuclei) including serotoninergic neurons in the raphe nucleus, norepinephrine neurons in locus coeruleus and glutamate neurons in the pedunculopontine nucleus. While oscillatory centres are isolated inter projections allow for interaction that can cause patterns to occur at the same time. Own depiction inspired by (Brown et al., 2012, p. 1099).

Thalamus is considered a relay for ascending signals in the awake state. It shows that certain nuclei that act as neural oscillators especially under certain conditions, most notably sleep. "During these states, the behavior of thalamic cells is characterized by long-lasting hyperpolarizations and phasic burst discharges recurring rhythmically" (Steriade and Deschenes, 1984, p. 21). Chirurgical removal of thalamus in cats was found to lead to a decrease

of the amount of non-REM sleep from 38% to 11.8%. In contrast diencephalic cats still showed sleep spindles (Montagna, 2005). Further support comes for example from fatal familial insomnia a deadly neurodegenerative disease. Findings indicate that thalamic atrophy causes a lack of sleep spindles and delta sleep which implies that "thalamus is the origin of slow wave sleep" (Montagna, 2005, p. 339).

Thalamic nuclei contain neurons that oscillate in the rhythms of slow wave highlighting its role for the regulation of sleep. Evidence suggests, however, that Rostral Midline Thalamus (RMT) acts as a relay for ascending arousal signals that originate from the reticular formation and abolish slow waves. Stimulation of the midbrain reticular formation in cats suppresses slow thalamic rhythms of hyperpolarizing episodes (Steriade and Deschenes, 1984). RMT is part of the nonspecific thalamic system. It contains nuclei that project to cortex in a spatially unspecific manner. While specific roles can be attributed to some cores one can assume RMT to alter the excitability of cortical neurons in a spatially rather unspecific way. (Vertes, Linley, and Hoover, 2015). Phasic desynchronization of the neocortex could only be observed upon stimulation of the midline thalamic area in cerveau isolé preparations of cats (Kawamura and Domino, 1968). Rostral midline thalamus relays signals of the ARAS that abolish slow waves.

Lateral posterior nucleus: Source of delta oscillations

While it was previously found that thalamic delta waves are absent in diencephalic cats where cortex is surgically disconnected from lower structures (Villablanca, 2004), Dossi et. al (1992) identified thalamocortical slow waves in the posterior lateral posterior nucleus of thalamus (LPN) that show delta oscillations (here: 0.5 - 4 Hz) even after dissection of related cortical areas. Intracellular recordings show highly rhythmical oscillations in membrane potential at around 0.5 Hz. These oscillations occur spontaneously. When exceeding a certain threshold each of these oscillations was found to generate exactly one action potential at peak depolarization. Moreover, it was shown that self-sustained delta oscillations can be elicited by electrical stimulation in short rhythmic pulses (Dossi, Nunez, and Steriade, 1992). These findings (1) clearly that LPN is a thalamocortical centre that generates delta waves and (2) that rhythmical excitation entrains neurons to exhibit a delta rhythm

themselves.

More recently the T-type calcium channels have been found to play a key role in thalamocortical circuits that generate slow waves in the delta range. EEG delta waves are practically absent during NREM sleep in knockout mice that lack the alpha G1 subunit of named calcium channel. Moreover, the duration of NREM sleep is generally reduced (Lee, Kim, and Shin, 2004). However selective modification of T-type calcium channels in RMT were found to have similar effects (Brown et al., 2012). This potentially indicates an abolishing effect due to changes in the thalamic sites of the ARAS.

As thalamic cores and cortex are strongly connected it was argued that they represent a common functional unit for the generation of delta waves. The circumstance that rhythmical stimulation elicits delta waves indicates that interactions between oscillations in thalamus and cortex exist. Potentially they bind activity in thalamocortical networks. However, the oscillators that produce slow waves in the delta range rely in thalamus.

Thalamic reticular nucleus: Generator for sleep spindles

Another thalamic nucleus is considered the source of sleep spindles. Sleep spindles manifest as patterns of damped oscillations in EEG. Sleep spindles are well visible in the frequency band between 7 and 15 Hz (Niethard et al., 2018). These patterns in EEG arguably arise from synchronous firing of cortical pyramidal cells. It is known however that sleep spindles originate from the thalamic reticular nucleus (Lüthi, 2014). Thalamocortical sleep spindles are considered to be a switch for the transition between light and deep sleep (Montagna, 2005). In many cases they cooccur with activity of cortical cells measured by two photon fluorescence microscopy (Niethard et al., 2018). The reticular thalamic nucleus is considered the pacemaker for sleep spindles that interact with slow waves.

Hippocampal formation: Origin of sharp wave ripples

Another area in the brain that is known to act as a neural oscillator resides in the hippocampal formation. Hippocampus represents the oldest part of cortex and exhibits a highly structured nature that has been extensively studied. An important feature of the organization of hippocampus is the overall flow

of signals that follows the scheme of the tri synaptic way. Signals from entorhinal cortex travel in circular patterns through hippocampus. Activation propagates from entorhinal cortex to the dentate gyrus, subsequently to the CA3 subfield, via the Schaffer collaterals further to subfield CA1 and finally back to the entorhinal cortex. This network topology is incorporated in spiking neural networks that can reproduce important features of hippocampal sharp wave ripples (Aussel et al., 2018).

Hippocampal sharp wave ripples can be produced in vitro. Long term potentiation of neurons that form the recurrent networks that include subfield CA3 is known to facilitate the generation of hippocampal sharp wave ripples. Repeated high-frequency stimulation of a particular area in subfield CA1 induces long term potentiation and enables short wave ripples both in area CA3 and CA1. These findings do not only indicate the source of origin of hippocampal sharp wave ripples but also its involvement in processes of memory formation (Behrens et al., 2005).

Neocortex: Source of neocortical slow waves

Neocortical slow waves occur spontaneously during deep sleep and deep anaesthesia in irregular rhythms with a frequency of one Hz and below. Differences have been found for ketamine induced anaesthesia and urethane where frequencies were found to be slightly lower (Steriade, Nunez, and Amzica, 1993). Neocortical slow waves have been described as recurring bursts of action potentials of neurons in several regions of cortex. Simultaneous acquisition of electrocorticograms (ECoG) shows that these bursts cooccur with an oscillation in the electrical potential on the cortical surface (Steriade, Nunez, and Amzica, 1993). Arguably these oscillations relate to the neocortical slow waves [$< 1\text{Hz}$] that can be measured using EEG during deep sleep. Simultaneous ECoG and widefield fluorescence imaging shows that up states typically cooccur with several oscillations of the ECoG potential (Stroh et al. 2013; see figure 2.1).

Simultaneous recording of ECoG and local field potentials (LFP) in the form of a electrothalamogram indicates the presence of a corresponding thalamic signal (Steriade, Nunez, and Amzica, 1993). The hypothesis that neocortex contains networks that act as a neural oscillator has been confirmed both empirically and by means of simulation (see section 2.2). However, it was

also found that optical stimuli and the resulting signal that originates from the retina are suitable to elicit slow waves. Besides optogenetic stimulation of the lateral geniculate body, the thalamic relay for signals from the retina, causes slow waves. Neocortical slow waves can hence not only arise because of random noise that manifests as spontaneous firing but can also be triggered by perceptual inputs and excitatory projections from subcortical sites. Moreover, it was shown that slow waves evoked in cortex strictly precede a signal that can be measured in thalamus. (Stroh et al., 2013). Taken together this indicates that cortex is the site of origin for this type of slow waves. Oscillations arguably arise spontaneously while the interaction with other signals can determine the precise time of the occurrence of neocortical slow waves. Two photon fluorescence microscopy reveals a differential behaviour of different neurons during up states of slow wave anaesthesia. It shows that neurons do not all behave in the same way but peak activity cooccurs with sleep spindles only for some neurons. In average the fluorescence signal correlates with slow waves measured using ECoG. As mentioned above the electrophysiological response does however not directly reflect the mean signal. Different neurons have specific response properties and cooccur with other oscillations in the brain in a selective manner (see also 2.5).

Interaction effects

Interaction effects between signals that arise from thalamus and those in cortex have been identified. Thalamus is evidently the source of sleep spindles and delta waves, the most important patterns of slow wave sleep. However, it shall be mentioned that thalamus is strongly interconnected with cortex. Electrical stimulation of the reticular core of thalamus was found to cause an increased in amplitude of delta waves in hippocampus. In contrast rhythmical stimulation of cortical area 7 evokes periodic oscillations in thalamic neurons that sustain over extended periods of time after stimulation offset. The resulting thalamic rhythm can in return enhance synchronization (Steriade and Deschenes, 1984, p. 21). This finding indicates not only that entrained rhythms exist in thalamus but also that oscillations in thalamus and both archicortex and neocortex strongly relate to each other.

Sleep spindles, hippocampal sharp wave ripples and neocortical slow waves are arguably not fully independent. Slow waves predominantly occur phase

locked to sleep spindles (Demanuele et. al. 2017). The spindle amplitude is correlated ($r = .3$) with the df/f signal in wake active cells (Niethard et al., 2018). A weaker yet significant correlation is found for wake inactive cells. The cooccurrence of slow oscillations and sleep spindles is also correlated with effects on the calcium fluorescence. A higher percentage change can be observed when both signals coincide as compared to the case of sleep spindles alone being present during a slow wave in calcium fluorescence (Niethard et al., 2018). Contingencies between hippocampal sharp wave ripples and slow waves and their role for memory consolidation are discussed in the next section.

Neocortical slow waves can be perceptually triggered and evoked by optogenetic stimulation of subcortical areas. Stroh et al. (2013) found that both the presentation of optical stimuli and optogenetic stimulation of the lateral geniculate nucleus (LGN) can cause neocortical slow oscillations. The LGN is the thalamic relay for visual information that originates from the retina and projects to visual area 1 in occipital cortex. The circumstance that slow waves can be triggered by signals that originate from areas other than cortex highlights potential interaction effects with other oscillations in the brain.

Figure2.1 illustrates the location of oscillatory nuclei which evidently play a role in slow wave sleep and shows the ventral and dorsal pathway of the ascending reticular activation system. The SCN that arguably plays an important role in the regulation of sleep according to the circadian cycle is additionally indicated. Note that oscillatory centres in the rostral medulla that orchestrate breathing during sleep are not indicated (Kubin, 2019).

While the named structures are arguably the source of the respective oscillation it must be noted that signals interact. They do not occur fully independently. Up and down states of neocortical slow waves arise in cortex while they can be caused by subcortical afferences. Empirical data indicates that oscillations in archicortex and thalamus are more or less tightly bound to neocortical slow waves (Niethard et al., 2018). The presumed role of cortico-hippocampal synchrony for memory consolidation is discussed in the next section.

2.5 Sleep slow waves and memory consolidation

A proposed function of slow waves is to "bind together" (Brown et al., 2012, p. 1110) several oscillatory patterns during sleep. Moreover, it was argued that slow waves represent an important mechanism for memory consolidation. According to the hippocampal-neocortical dialogue model of slow waves, the interaction of hippocampal sharp wave ripples and neocortical slow waves fosters memory consolidation (Buzsáki, 1996): Recently it was shown that generating neocortical slow waves in prefrontal networks such that they are coupled to the occurrence of sharp wave ripples in the hippocampus increases the performance of rats in a memory task (Maingret et al., 2016). Coherently, a correlation of slow wave activity and the brain-derived neurotrophic factor was found for humans (Duncan, 2013). Spontaneously occurring slow waves arguably play an important role for memory. The hippocampo neocortical dialog model states that memory acquisition is a two-stage process. Accordingly (1) associations between sparse perceptual codes and the internal world are formed in hippocampus whereas (2) memory replay occurs during slow wave sleep and establishes long term memories in the interaction with neocortex. A further hypothesis is that information is gathered sequentially during theta oscillations and replay occurs during sharp wave population bursts (Buzsáki, 1996). Although not all hypotheses can be confirmed important key elements of the model are well supported by empirical findings.

Entorhinal cortex represents the neocortical interface to hippocampus. It provides both the main input and is the main target area of hippocampal projections (Buzsáki, 1996). Entorhinal cortex resides on the highest hierarchy level of the Van Essen Diagram (Felleman and Van Essen, 1991). Visual information can be assumed to be processed in a hierarchical manner along the ventral pathway. Whereas response properties in early visual cortices relate to physical features of the visual percept such as simple shapes that occur in a specific receptive field, neurons evidently code for more abstract concepts in higher areas. Famous examples are the parahippocampal place area (PPA) or the fusiform face area (FFA) both of which reside in close proximity of the hippocampal formation (Coggan, Baker, and Andrews, 2019). It can be deemed certain that that hippocampus receives a highly processed perceptual code.

Hippocampus exhibits a well-defined structure that contrasts with neocortex and includes circular pathways of projections that allow for recurrent activity (Graham, Cutsuridis, and Hunter, 2010). Electrophysiological studies of hippocampal circuits revealed that long term potentiation occurs in hippocampus. High frequency stimulation causes long lasting effects highlighting the role of hippocampus for learning (Behrens et al., 2005). Simulation studies indicate that hippocampus acts as an auto associative memory (Graham, Cutsuridis, and Hunter, 2010). Strikingly specific protocols of high frequency stimulation were not only found to cause long term potentiation but have recently been shown to act as a trigger for hippocampal sharp waves (Behrens et al., 2005).

While hippocampus plays an important role for the acquisition of knowledge it is known that neocortical sites encode learned contents ⁴. The entrainment of cortical sites by previously acquired hippocampal codes during sleep is postulated by the neocortical hippocampal dialogue model and can be demonstrated empirically.

Empirical data shows that memory replay occurs during sleep both in hippocampus and the associated cortical sites. Both areas contain neurons that code for the learning experience. Ji and Wilson (2007) investigated contingencies between behaviour and slow wave sleep to study the interaction between hippocampus and neocortex in the acquisition of long term memories. They investigated the response properties of neurons in rats in an experimental paradigm that includes maze running in an eight shaped maze. Place cells were identified that fire for different regions of the maze. Depending on the direction of running different patterns in the neural response show. The sequence of peak activities of the recorded neurons codes for the direction in which the rat passes through the maze. It was found that these sequences are replayed in hippocampus during slow wave sleep. Most interestingly, however, memory replay did not only take place in archicortex but neocortical signals appeared to be correlated. Neocortical place cells were also active. Moreover the same sequences of neural responses are measurable in hippocampus and neocortex which indicates that memory replay occurs during sleep (Ji and Wilson, 2007).

⁴Only moderate effects of retrograde amnesia exist in patients with hippocampal lesions indicating that declarative memory formation but not retention is impaired (Spiers, Maguire, and Burgess, 2001). The performance of rats with hippocampal lesions is impaired both for spatial learning and novel object rECOGnition tasks but not in motor skill learning (Gould et al., 2002).

Evidence further suggests that the synchrony between slow waves and hippocampal sharp wave ripples during sleep enhances learning. This was demonstrated in a stimulation paradigm where slow waves are triggered such that they coincide with sleep spindles measured in the hippocampal formation (Maingret et al., 2016). It is not fully understood why increasing the synchrony between two signals that can oscillate independently fosters memory consolidation. One may speculate, however, that hippocampal signals can change synaptic weights of neocortical populations only if they trigger action potentials. Hence a simultaneous up state would be required.

As hippocampal memory replay is associated with specific neocortical neurons one may hypothesize that signals such as sharp wave ripples could trigger slow waves that incorporate distinct populations which correspond to the learning experience. Memory consolidation would accordingly be achieved by strengthening the synaptic weights of (1) the memory engram in neocortex by repeated activation of the respective synapses and (2) the associations between these neurons and sparse hippocampal codes.

As mentioned above source modelling of sleep slow waves indicates cingulate fibre trajectories (Bernardi 2018). Because of its high spatial resolution fluorescence microscopy can provide more fine-grained distinctions and may potentially reveal trajectories of neural signal transduction during slow wave anaesthesia. This highlights the importance of methods that allow to capture the variance of temporospatial patterns of neural slow waves.

2.6 Neocortical slow waves: Towards a working definition

A distinction between slower and shorter waves has already been made in the pioneering electroencephalographic study almost a century ago (Berger, 1929, p. 550). Shortly later the term delta wave was coined to describe oscillations in the recorded voltage in the respective frequency band. Delta waves are defined for a frequency of 1 to 4 Hz by some authors (Kubin, 2019) while others define the delta range for oscillations between 0.5 to 4Hz (Dossi, Nunez, and Steriade, 1992). The term slow wave is also used to describe oscillatory patterns in EEGs in the delta range. "Slow-wave activity (SWA) is defined as the EEG power in the slow wave frequency band" (Furrer et al.,

2019, p. 1). It shows that the term "delta wave" is sometimes used as a synonym for "slow wave". The term slow wave is rather loosely defined, and it is hence important to give a clear account of what is understood as a slow wave here.

Slow waves refer to a pattern in EEG but also to distinct neural phenomena. Depending on the context slow waves describe as a pattern measured with one method or oscillations that can be recorded in a methodologically rather agnostic way. For example changes in the spike rates of neurons or fluorescence signals are also referred to as slow waves (Jercog et al., 2017; Stroh et al., 2013). This shows that the term slow wave is used in relation to the neural phenomenon, its functions and its signatures that can be measured using various methods.

Slow waves in the wide sense are both neocortical slow waves and thalamocortical slow waves in the delta range. For example, Celotto et. al (2020) denote neocortical slow oscillations as slow waves. Furrer et al. (2019) use the term as a synonym for delta waves instead. As explained in the previous sections both phenomena can occur independently from one another. It is hence advisable to use distinct terms. Steriade et. al (1993) suggested the label neocortical slow oscillation. It was noted, however, that the up states and down stated do not necessarily appear in a rhythmical pattern (Brown et al., 2012). In addition, the transition to an up state appears as a slowly travelling wave. As the term is more descriptive this phenomenon is hence referred to as neocortical slow wave. In contrast thalamocortical slow waves relate to slow waves in the delta band (1-4 Hz). Sleep slow waves show more irregular patterns in EEG and could potentially include signatures of both neocortical slow waves and thalamocortical slow waves in the delta range (Steriade, Nunez, and Amzica, 1993).

Slow waves are short periods of above baseline activity that occur in bistable states such as deep sleep and anaesthesia which are characterized by reduced neural excitability. Slow waves reflect the up states that are interlaced with down states of neural activity (Jercog et al., 2017). They are dynamic patterns of recurrent activation of large potentially distinct populations of neurons. Slow waves can differ with respect to the pathway of neural flow that show especially in early stages of up states and with respect to the set of recruited cells where recurrent activity prevails. They appear as propagating waves in widefield and two-photon calcium imaging in vivo (Celotto et al., 2020;

Niethard et al., 2018).

Slow waves are dynamic patterns of flow. The rising phase of slow waves can be understood as a runaway process: If activity exceeds the threshold they fire and cause postsynaptic potentials which can elicit action potentials in the target neurons (Nghiem et al., 2018). Travelling waves can arguably be observed because of the spatial arrangement of neurons in cortex where close sites are preferably connected more strongly. Traveling waves can even be observed in neocortical slices in vitro (Wu, Huang, and Zhang, 2008). Cortex is known to be of a highly recurrent nature (Gămănuț et al., 2017). Arguably this is why one can observe extended periods of activation as these neurons can be assumed to directly or indirectly project back to the one that initially fired. Hence, slow waves can reveal regions of high functional connectivity. However also cingulate fibre trajectories were identified in EEG during sleep (Murphy et al., 2009). Neocortical slow waves could also travel through cortex via structured fibre bundles. Patterns of neural flow could result from signals that travel via fibres of cingulum that connects entorhinal cortex and the bordering hippocampus with neocortical sites.

Neocortical slow waves can be understood as a process that includes synchronization with other neural oscillations. If hippocampal sharp wave ripples correlate with cortical up states one may speak of a hippocampo neocortical slow wave. Thalamocortical slow waves arguably interact with the networks that cause neocortical slow waves. Analogously one could form subcategorizations for slow waves that incorporate deviant sets of connected neurons.

The exact slow wave frequency depends on the method for data acquisition. Here data from widefield fluorescence imaging is analysed. This raises the question how slow oscillations in calcium imaging differ from their counterpart in EEG or ECoG. The simultaneous acquisition of ECoG and wide field GCaMP imaging reveals that up states cooccur with oscillations in the cortical potential. Slow waves in the mean fluorescence signal cooccur with slow waves in the electrophysiological recording (Stroh et al., 2013). The respective correlation could also be demonstrated on the basis of individual cells using two photon imaging (Niethard et al., 2018). It shall be noted however that the frequencies of neocortical slow waves differ between ECoG and widefield fluorescence. Lower frequencies could potentially be the result from smoothing due to lower sampling rates and the required exposure time

in fluorescence imaging or an involvement of distinct populations of neurons at different points in time.

Slow waves can have several subsegments. As slow waves are understood as short periods of above baseline activity, they can incorporate multiple oscillations. These stages could potentially relate to distinct neural events. The circumstance that slow waves can include several oscillations is especially important for the detection and separation of events. It means, however, that events could not be separated based on local minima alone (Celotto et al., 2020). Nonetheless, it is reasonable to assume that multi peak slow waves exist.

Conceptualizing slow waves as above baseline activity bears potentials for revealing the temporal dynamics of slow waves that incorporate several stages. It also means that new methods are required for the analysis the dynamic of slow waves. Slow waves can be defined in various ways. They are up states that may include several oscillations and have distinct properties that include dynamical pathways of flow and the synchrony with other oscillations in the brain.

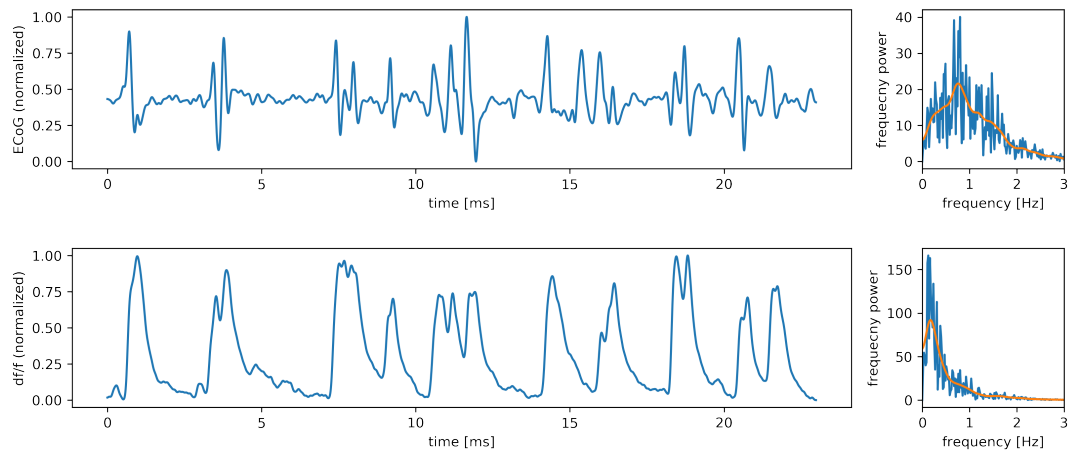


Figure 2.2: Frequencies of slow waves differ between measuring techniques. Data was recovered from supplementary figure 4A, Stroh et al. (2013) for secondary analysis. Signals are smoothed using a gaussian filter and subsequently normalized. Baseline correction was applied for the hemodynamic calcium signal (lower left). The resulting noise reduced signals were investigated with respect to the frequencies present. Upper row: The normalized Electrocorticogram (left) and the frequencies power revealed by Fourier Transform (right). Lower row: The normalized signal change of the hemodynamic response (left) and the corresponding frequency spectrogram (right). The frequency power is plotted in blue whereas a smoothed version is plotted in orange. It shows that the peak frequency of the hemodynamic signals relies below 0.2 Hz whereas the peak frequency of the calcium signal is above 0.7. Note also that slow waves of both signals are aligned but several ECoG oscillations occur during a hemodynamic event.

Chapter 3

Methods

3.1 A new approach to track intracerebral blood flow

Widefield fluorescence imaging has a typical sampling rate of 25Hz (Celotto et al., 2020). However, the dataset at hand was recorded at 100Hz. High-speed recordings bear potentials for the analysis of neural signals beyond the frequency of neocortical slow waves. The high spatial resolution could in principle reveal patterns on a sub-millimetre-scale. New methods must be established to identify the origin of high frequency components. This is especially important because widefield fluorescence recordings are confounded with an error that results from the hemodynamic autofluorescence. The approach presented in this section indicates that high frequencies in the df/f signal relate to hemodynamic effects. Arguably high frequencies mainly stem from a signal that results from clusters of oxygenated blood which flow through intracerebral blood vessels of various size.

The approach presented here allows to measure intracerebral blood flow without the need for the injection of tracers. Typically, microbeads are used to detect the flow rates and speed of intracerebral blood (Kim and Shin, 2019). The study of intracranial blood flow bears potentials for a better understanding of pathologic conditions and basic neurobiological functions of the brain. For example, it was shown that the micro vessel density decreases in brain tumours and characteristic changes in the haemoglobin concentration can be observed in mutated tissue (Lee et al., 2014). However intracerebral blood flow is also addressed in by neuroscientists in the study of neurometabolic and neurovascular coupling (Devor et al., 2012). The circumstance that the blood oxygen level dependant (BOLD) contrast is extensively used in the study of the human brain fMRI further highlights the relevance of neurometabolic effects. New approaches to track the blood flow in the

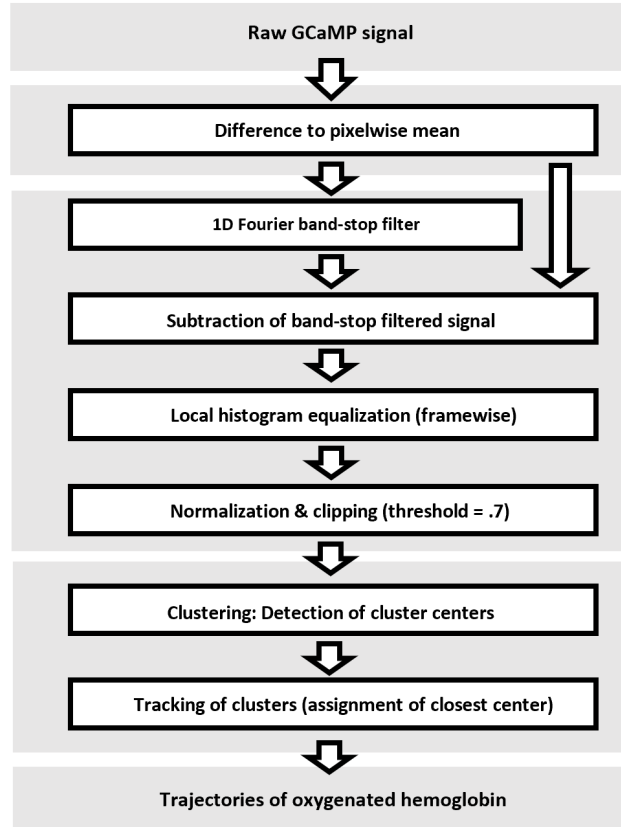


Figure 3.1: Processing pipeline for the detection of bloodflow

brain could help to better understand the interaction between the activity of neurons and hemodynamics.

Several processing steps were employed to determine what high frequency components of the fluorescence signal relate to (see 3.1). First the mean image was calculated and subtracted from each frame of the recorded videos. The signal in time was then band stop filtered and the difference to the original signal was calculated. Band stop filtering was achieved using 1D Fourier Transform. The signal in time for each pixel is (1) transformed to the Fourier domain (2) the frequency components in the desired range are set to zero and (3) inverse Fourier transform is applied. Adaptive histogram equalization was used to improve the contrast of each frame after clipping the values below a given threshold. In the resulting videos clusters of bright foreground pixels move on decisive trajectories (see Figure 3.3).

Cluster tracking is used to measure the pathways of these temporospatial patterns. Objects in binary images that are potentially connected are often labelled using watershed distance transform (Arganda-Carreras and Legland,

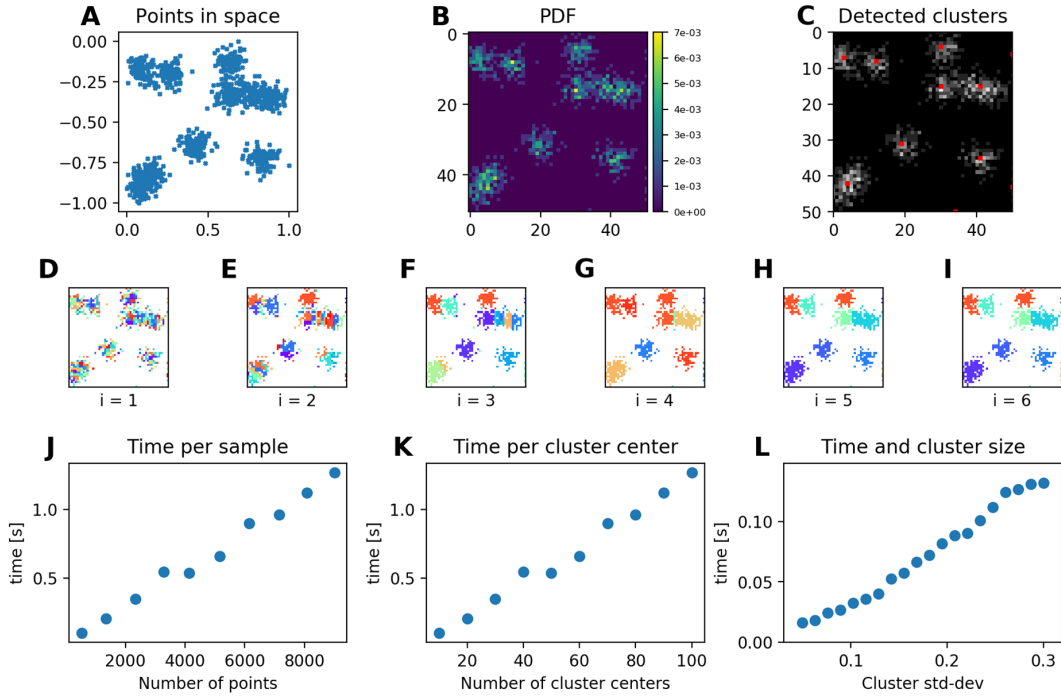


Figure 3.2: A mean shift approach for clustering pixels. After clipping the pre-processed hemodynamic signal, groups of bright, rather isolated foreground pixels are visible. These pixels can be considered as evidence for the presence of oxygenated haemoglobin particles. To detect the location of named clusters of pixels a variation of mean shift clustering was implemented that works with density matrices. Panel A: A distribution of points in \mathbb{R} . Cluster centers were sampled using a 2D gaussian. For each cluster centre points were added using a second gaussian probability distribution centred at the respective location. Panel B : A 2D histogram of the distribution in panel A indicating the probability density function. Panel C: The detected cluster centres. Panels D-E: Assignment of pixels to clusters for the first seven iterations beginning with $i=1$. After iteration seven convergence is achieved. Panel J: Time per sample. Panel K: Time per cluster Panel L: Time per cluster size.

2016)¹. As the data (1) was not binarized but clipped and (2) it has a low relative resolution which results in a rough outline of foreground pixels that does not allow for the computation of meaningful watersheds a different approach was used. The aim is to detect clusters of nearby foreground pixels. The clipped images were interpreted as probability density functions that indicate the presence of oxygenated haemoglobin. Clusters are detected using this 2D array as the input. Each nonzero value is added to the position in an output array that corresponds to the centre of gravity of a neighbourhood

¹Distance transform assigns the value to the closest background pixel to each foreground pixel. Different algorithms exist that allow for fast approximations. The resulting image represents a heightmap if the distance values are interpreted as depth. A simple flooding algorithm can be used to determine the watersheds: A simulated rise of the water level fills basins in the heightmap. The borders between adjacent basins are the watersheds that separate the detected objects.

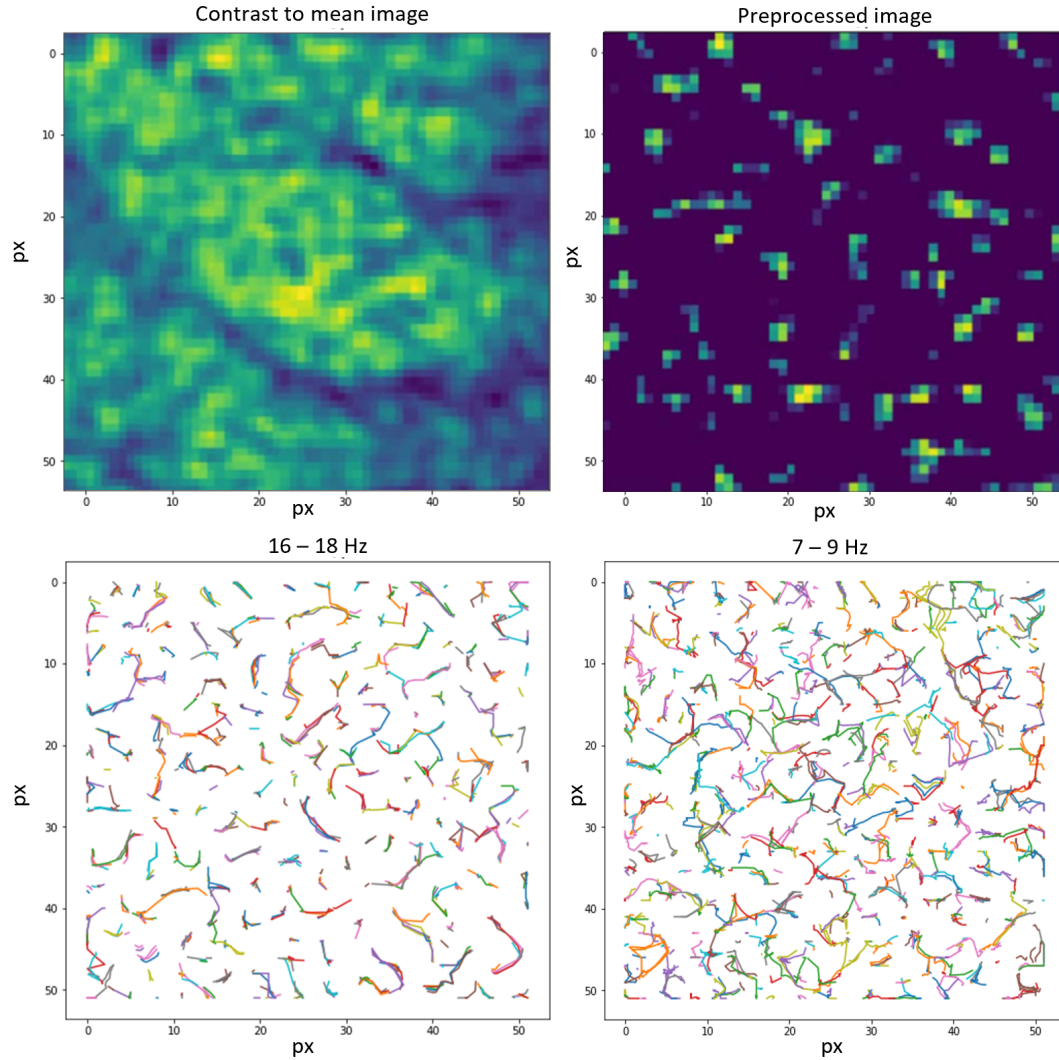


Figure 3.3: Cluster tracking reveals trajectories of oxygenated hemoglobin.
 Upper left: A sample frame for the original contrast to the pixelwise mean.
 Upper right: The pre-processed frame after application of clipping. Lower left:
 Detected trajectories for filtering of frequencies in the range of the heartbeat.
 Lower right: Detected trajectories of bloodflow for filtering of low frequencies.

See also Figure 3.2

around the respective pixel in the input. This procedure is repeated iteratively using the output array as the input. The centre of gravity relates to the weighted mean of the pixel coordinates along each axis where the density values are used as weights. Areas that converge to a common target location are assumed to relate to the same cluster. It is kept track of the original pixels such that the image can be labelled accordingly. The cluster centres are determined as the centre of gravity of each group. The algorithm stops if convergence is achieved or a maximal number of iterations reached. The environment for the computation of the centre of gravity could be a square or a

circular patch. To reduce the impact of distant points on the centre of gravity they can be weighted using a 2D gaussian. For the results shown in Figure 3.3 a simple rectangular patch was used. As the data is shifted towards the centre of gravity the approach can be considered a mean shift technique. Important properties were studied stochastically using simulated data. First cluster centres were sampled from a uniform distribution. Second data for each cluster centre was sampled from a second 2D gaussian function. A smaller standard deviation was chosen for the latter function such that distinct clusters form. Note however, that an overlap was not prevented. However, it was aimed for a sparse coverage of the resulting space to limit interaction effects due to overlapping neighbourhoods of pixels from neighbouring clusters.

Figure 3.2 summarizes the results. The computation of 2D histograms can be achieved in $O(n)$ as iterating over the data once is sufficient. As the size of this histogram can be chosen freely the computation time does not directly depend on the number of samples. Given that the algorithm converges, and clusters are far enough apart for the clusters to collapse independently (i.e. the neighbourhoods around the respective pixels of two neighbouring clusters never overlap) it can hence be assumed that it takes the same amount of time for each cluster in average. Hence a linear relationship between the number of clusters and the runtime can be assumed. The simulation confirmed this assumption (see 3.2K). Consequently, the number of samples also scales linearly with the processing time for the given sampling strategy. One may hence assume that the runtime scales linearly with the number of samples if they are arranged in small clusters with large spacings and the size of the neighbourhood is chosen accordingly. In this case the time complexity is $O(n)$.

Clustering is performed for each frame separately. The result is a list of cluster centres per frame. Tracking is achieved by assigning the closest cluster centre of the subsequent frame if the maximal distance is less than ten pixels. In principle other rules can be implemented. For example, the cluster size could be considered and only those clusters can be matched that are of comparable size. Alternatively, an objective function with several constraints could be defined and used to determine the correspondence between clusters. A comparable method for cluster tracking that employs mean shift clustering in colour-space employs kernels instead of the abovementioned

maximal distance rule (Kumar, Raja, and Gandham, 2020). As the approach was not used to study slow waves the simplest rule for tracking was used to demonstrate the feasibility of the approach.

It shows that particles move on decisive trajectories. These trajectories depend on the frequency used for band stop filtering. If band stop filtering is applied in the range of the heart rate shorter trajectories are detected and the clusters appeared to be larger. In contrast for higher frequencies a more filigree patterns can be observed. It can be hypothesized that these patterns relate to blood that travels at different speeds in vessels of different size. A more systematic study that compares trajectories revealed by the use of tracers could help putting these findings into perspective and test this hypothesis. Because of the presumed hemodynamic effect for high frequencies band stop filtering was used to reduce the impact of blood flow on the signal d in the main approach presented here.

3.2 Dense Optical Flow

Vector fields of pixelwise displacements that reflect the apparent motion between two subsequent video frames are called Optical Flow. Sparse Optical flow uses local features that are not necessarily present in every location of the images. Hence it yields sparse vector fields for which many values are undefined. In contrast Dense Optical Flow computes a motion vector for every pixel coordinate. Multiple algorithms exist that allow for the computation of sparse or Dense Optical Flow.

One class of algorithms is based on image gradients and uses iterative schemes to compute sparse or dense vector fields. Classical examples for algorithms that are still used today include the methods of Lucas and Kanade (1981) as well as the approach suggested by Horn and Schuck (1981). The approach by Lucas and Kanade (1981) depends on a linear approximation of the behaviour of a function $F(x)$ and $G(x) = F(x + h)$ in a local neighbourhood where h relates to a shift that is assumed to be sufficiently small. As Lucas and Kanade (1981) illustrate for the one-dimensional case the approach is inspired by the formula for the numerical derivative $F'(x) = [G(x) - F(x)]/h$ or respectively $F'(x) = [G(x + h) - F(x)]/h$ that can be rearranged to express the shift as a function of the difference of both curves divided by the slope of the unshifted version: $h = (G(x) - F(x))/F'(x)$. This formula

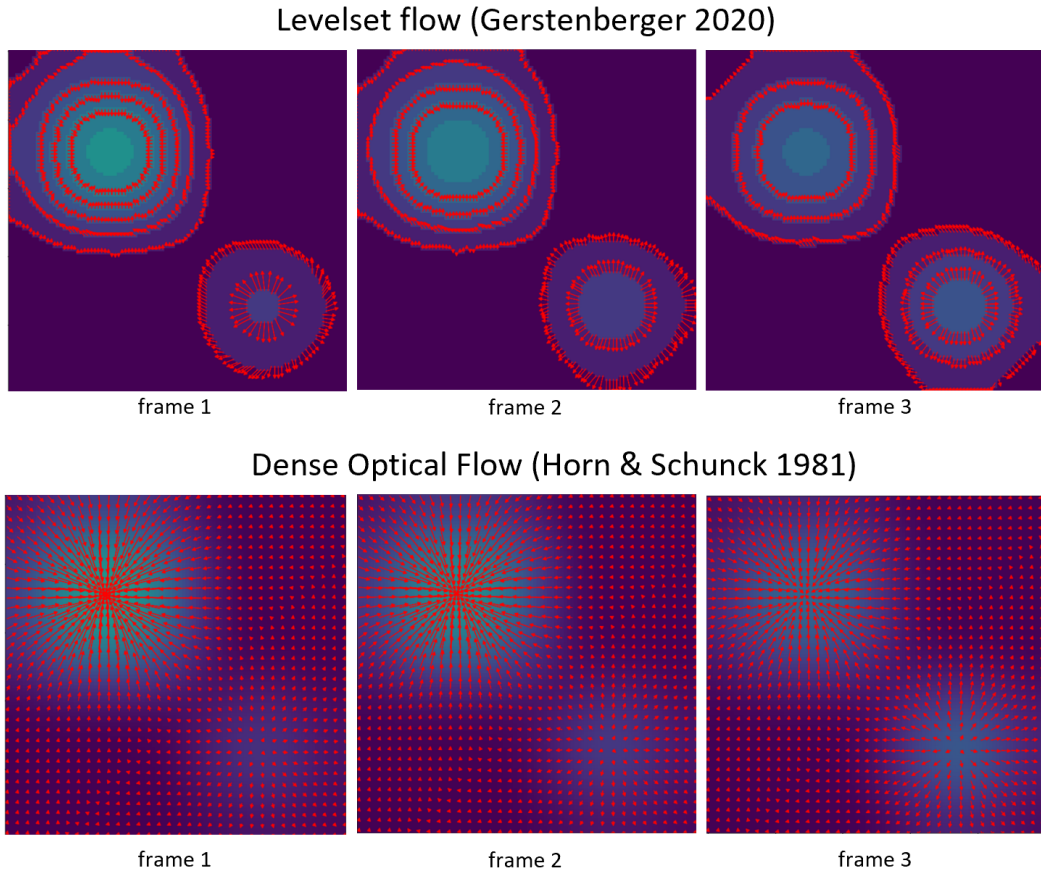


Figure 3.4: Levelsets and Dense Optical Flow

The results of an approach to track the outline of levelsets are plotted in the top row while Dense Optical Flow is plotted in the lower row. Note that only a subset of levelsets was used for the earlier approach. While Dense Optical Flow requires smooth inputs it detects similar yet dense vector fields. The movement of the wavefront of a slow wave can be represented as a binary sequence of frames. Dense Optical Flow captures the movement of multiple levelsets simultaneously and hence represents a more general approach.

yields a good estimate especially for small shifts. To improve the estimate, a weighted average is computed for multiple values of x in a local neighbourhood. A weighting term is used that increases the impact of values for which the slope of $F(x)$ is approximately linear. To further improve the detected displacement vector an iterative scheme is employed. The previous estimate for the shift is used to move F accordingly and determine the shift again for $F(x + h)$. The estimate is updated by adding the new approximation to the preliminary displacement. The two-dimensional form is largely identical to the one-dimensional case, however the weighting differs. As Lucas and Kanade (1981) method assumes a small shift between original image and shifted version and is based on spatial derivatives (i.e. the image gradient) it

requires smooth data. Moreover, the estimate for the shift is undefined when the gradient within a local neighbourhood is all zero. Hence it is often used in combination with approaches to detect salient features and compute displacement vector only for these locations in order to retrieve sparse vector fields.

Here we compute dense vector fields of Optical Flow using the method suggested by Horn and Schuck (1981). To a certain extent it is similar to the approach suggested by Lucas and Kanade (1981). By that it is meant that formula used to iteratively estimate the displacement vectors includes the spatial derivatives of the image as well. However, the term also includes the temporal derivative between the pixels of the two subsequent frames. Horn and Schuck's method computes Optical Flow using both the image gradient and the temporal derivative. Optical Flow is the result of minimizing an objective function that represents an energy functional. In analogy to the approach by Lucas and Kanade (1981) an iterative scheme can be derived.

$$d^{k=0} = \frac{I_t}{\alpha^2 + I_x^2 + I_y^2} \quad (3.1)$$

$$\begin{aligned} u^{k=0} &= -I_x d \\ v^{k=0} &= -I_y d \end{aligned} \quad (3.2)$$

The general form of the iterative scheme that is employed by the Horn and Schuck method is expressed by equation 3.4 and 3.3. The arrays of vector components U and V are initialized with zero. Hence the general form of the iterative scheme used by the Horn and Schunck algorithm reduces to equation 3.1 and 3.2 for the first iteration. Two special cases can be distinguished. If the temporal gradient is zero, the denominator and term d itself become zero. This means that also the vector components U and V are zero as d is multiplied with the image gradient and U and V are initialized to zero. This meets the intuition of Optical Flow. If a patch of brightness values is not shifted to a new location, there is no change in the intensity over time. Hence there is no apparent motion if the temporal derivative is zero.

In contrast, if the spatial gradient approaches zero the impact of a temporal brightness change on the estimated vector magnitude becomes greater. This is because the squared spatial derivatives are added in the denominator of d. Hence it scales inversely with an increasing spatial gradient. The estimate

for U and V linearly depend on d. It holds that $\lim_{I_x, I_y \rightarrow \infty} d = I_t / \alpha$. Typically a small value is used for alpha (here 0.04). If the brightness increases by a fixed value between pairs of images that either both have a soft gradient or a steep gradient the estimated Optical Flow will be different. This meets the intuition. In the case of a soft gradient differences in brightness between far apart areas are small. Hence, a small increase in brightness is sufficient to displace areas with a given grey value over large distances. Intuitively gradient based methods for Dense Optical Flow can be interpreted to indicate the displacement of grey values.

$$d = \frac{(I_x \bar{u}^k + I_y \bar{v}^k + I_t)}{\alpha^2 + I_x^2 + I_y^2} \quad (3.3)$$

$$\begin{aligned} u^{k+1} &= \bar{u}^k - I_x d \\ v^{k+1} &= \bar{v}^k - I_y d \end{aligned} \quad (3.4)$$

Besides classical approaches there are many other techniques that allow for the computation of Optical Flow ². These approaches are not necessarily based on gradients. Co-registration of patterns can for example also be achieved by retrieval and matching of scale invariant features (Zhang, Tsoi, and Lo, 2014). More recently deep neural networks have been proposed. Networks that employ regression layers and are trained in an end-to-end fashion to predict dense vector fields. While it was noted that domain specific overfitting must be addressed, they have been demonstrated to outperform other approaches for videos that depict natural scenes. The task of direct prediction of displacement vectors is typically addressed using Autoencoders for the transfer from the image domain to motion fields (Hur and Roth, 2020). Dense Optical Flow can be understood a nonlinear mapping from dense pixel arrays to vector fields.

In neuroimaging the spread of slow waves is typically measured using delay maps (Celotto et al., 2020). Local minima can be detected that indicate whether an event has already started for a point in time for a given discrete time interval. The result can be displayed as a binary video where the transition from positive to negative values reflects the position of the wavefront. Here it was aimed for a description of slow waves that can potentially incorporate several oscillations that may occur simultaneously and even overlap.

²For a comparative evaluation on the Sintel dataset see Max Planck Institute (2020)

Hence an approach was tested that can handle both binary wavefronts and level set flow.

The relationship between moving wavefronts and Optical Flow can be demonstrated using an approach that allows to track level sets. Level Set Flow computes displacement vectors for binary level sets. A vector field is computed in which vectors point towards the outline of the binary object. This is achieved by the computation of Distance Transform of the foreground and the background pixels of the target frame. The results are stored in a single 2D array. This representation can be interpreted as a scalar potential. The outline of the foreground pixels is detected in the source image. Then gradient descent is performed beginning at each of the coordinates of named pixels following the gradient of the scalar potential. Once a position is reached where the target matrix is false the procedure stops and is repeated for the next coordinate. The approach yields vectors that indicate the displacement of the outline of binary level sets.

It shows that Horn and Schuck's method for Optical Flow computes vector fields that resemble the movement of level sets. However sufficient smoothing is required. The method of Horn and Schunck (1981) has already been demonstrated to be useful for the characterization of temporo-spatial-patterns in fluorescence recordings (Townsend and Gong, 2018). Neuroimaging data represents non-textured data, can satisfy the smoothness requirements and hence be used for the computation of Dense Optical Flow using Horn and Schucks method. Dense vector fields are required for the application of Helmholtz Decomposition.

3.3 Helmholtz Decomposition

Vector fields can be used to describe various physical phenomena including fluid dynamics or magnetic flux but also the dynamics of spreading waves of neural activity. Dense vector fields of displacements can be computed from fluorescence recordings using Dense Optical Flow (Townsend and Gong, 2018). Patterns in these vector fields can be used to characterize the way neural signals travel in cortex during slow wave sleep and anaesthesia. Townsend and Gong (2018) suggest a kernel-based approach to detect several local and global features. A more general approach that allows to study fundamental properties of vector fields is Helmholtz Decomposition.

Smooth vector fields can exhibit a complex structure that can be described in several ways. There are properties such as the field strength that can be computed for every vector individually. Besides a distinction can be made between local patterns that relate to a subset of neighbouring vectors and global features that describe the vector field as a whole. Local patterns include inward spirals or patches of vectors that point towards a specific location or line surrounded by them. Townsend and Gong (2018) describe the latter two examples as stable nodes and saddles. In contrast unstable nodes and outward spirals relate to patterns where vectors point away from a specific location. An example for a feature that describes the vector field as a whole are plane waves in velocity fields that describe the average normalized speed (Townsend and Gong, 2018). These patterns may occur in isolation, but they can also co-occur and create complex structures of potentially overlapping features. For example spirals can be expressed as an addition of a diverging vector field and one with nonzero curl (CEDMAV, 2020). This raises the question what the fundamental components of vector fields and their characteristic properties are.

$$\operatorname{div} \vec{F} = \frac{\partial P}{\partial x} + \frac{\partial Q}{\partial y} \quad (3.5)$$

$$\operatorname{curl} \vec{F} = \frac{\partial Q}{\partial x} - \frac{\partial P}{\partial y} \quad (3.6)$$

Two important local properties of vector fields are curl and divergence. "Divergence is an operation on a vector field that tells us how the field behaves toward or away from a point" (Strang and Herman, 2018). Areas where a vector field contains sources or sinks have nonzero divergence. To compute divergence for a 2D vector field (1) the numerical derivative of the 2D array of X components is retrieved along the X axis, (2) the numerical derivative of the respective array of Y components is computed along the Y axis and (3) the resulting 2D scalar arrays are added. In other words divergence relates to the sum of the partial derivatives of the vector components with respect to the vector dimension they express (Equation 3.5). The computation of curl is based on partial derivatives of the vector components as well. However, curl is defined as the difference between the partial derivative of the Y-components (Q) with respect to X and the partial derivative of the X-components (P) with respect to Y (Equation 3.6). An example for a vector

field that has nonzero curl is $\mathbf{F}(x,y)=[y,-x]$. It shows circular flow and has zero divergence.

Helmholtz Decomposition allows to decompose vector fields into a curl

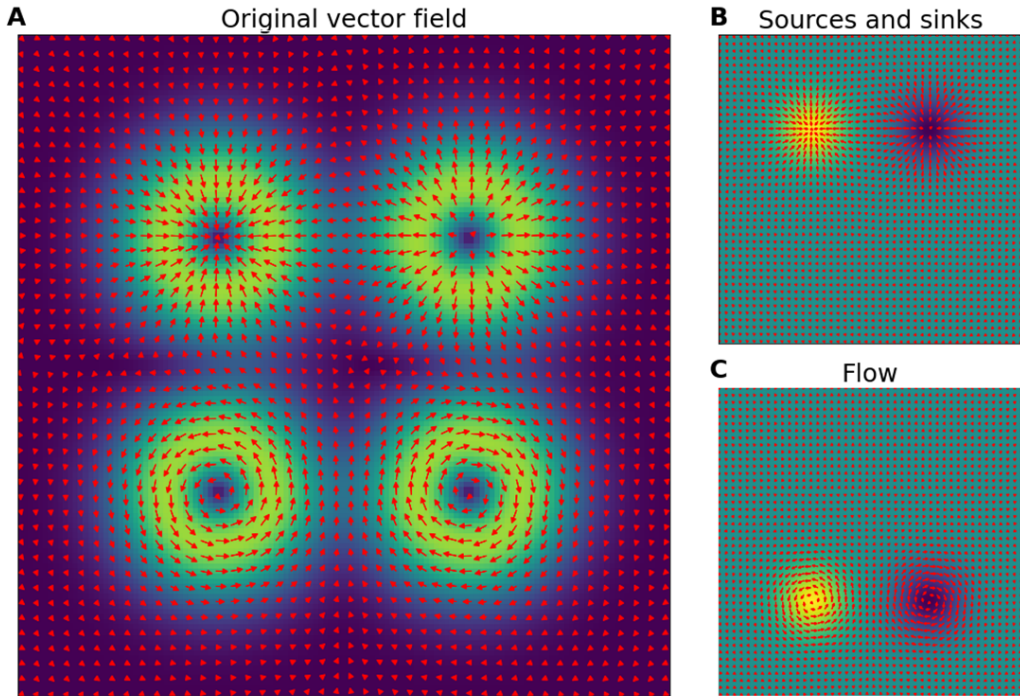


Figure 3.5: Helmholtz decomposition of a sample vector field.

Panel A: A vector field that contains a sink (top left), a source (top right) as well as areas with positive and negative curl (bottom left and bottom right). The field strength is plotted in the background. Panel B: The distribution of sources and sinks. The scalar potential of the curl free component is plotted in the background. Note that yellow tones indicate positive values while blue tones indicate negative values. The gradient field is plotted in the foreground. Panel C: The flow component. The scalar field is plotted in the background where blue tones relate to negative and yellow tones to positive values. The vector field $\nabla \varphi_{div=0}$ is plotted in the foreground.

free and a divergence free component. It is used in several disciplines to study various phenomena. Helmholtz-Decomposition can be used to model weather phenomena, ocean currents, electromagnetism, geophysical phenomena but it is also used in computer graphics and computer vision (Bhatia et al., 2012). Applications in neuroimaging exist as well. Helmholtz Decomposition has been used in combination with Dense Optical Flow of heightmaps that indicate cortical growth captured by MRI to determine growth seeds in the neonate brain (Lefèvre et al., 2009).

The fundamental theorem of vector calculus (Helmholtz-Theorem) states that every vector field can be expressed as the sum of a curl free and a divergence

free vector field if it is sufficiently smooth and decays rapidly. The definition is given by Equation 3.7. The curl free vector field relates to the distribution of sources and sinks. In contrast the divergence free component is also referred to as flow. Helmholtz Decomposition is used to retrieve these two components for a given vector field. This is achieved by an approximation of the scalar potential of the curl free component and a scalar field for the flow. The respective vector fields are defined as $\nabla\varphi_{curl=0}$ and $J\nabla\varphi_{div=0}$. Sources have negative values in the scalar potential of the curl free component while sinks have positive values. In contrast areas with rightwards curl and leftwards curl have negative and positive values in the scalar field of the divergence free component. Figure 3.5 illustrates the decomposition of a vector field that contains a source and a sink as well as areas with rightwards and leftwards curl in distinct areas.

$$v = \nabla\varphi_{curl=0} + J\nabla\varphi_{div=0} \quad (3.7)$$

There are several ways to compute Helmholtz Decomposition. Most approaches are based on the minimization of an energy functional. However, Machine Learning can also be employed to compute the divergence free component and the curl free component. For example a radial basis function (RBF) can be trained to learn the mapping between a vector field and the curl free or the divergence free component. Named approach employs statistical learning and is suitable for potentially noisy data (Bhatia et al., 2012). Here natural Helmholtz Decomposition is used to decompose vector fields of Dense Optical Flow and retrieve the curl free component as well as the divergence free component (Bhatia, Pascucci, and Bremer, 2014).

Helmholtz Decomposition is applied on Dense Optical Flow. To illustrate the relationship between the change in brightness in the original signal and Helmholtz Decomposition of Dense Optical Flow the approach was applied on simulated data. Two sequences of frames were computed. The first signal represents a global brightness gradient with an increase in intensity over time. The second signal was generated by gaussian smoothing of a binary 3D array where the X and Y axis relate to space and the Z axis relates to time. This 3D array was initialized with zeros and two areas that represent a cuboid were filled with a positive value. A third signal was generated by the addition of both named signals. Optical Flow was computed subsequently

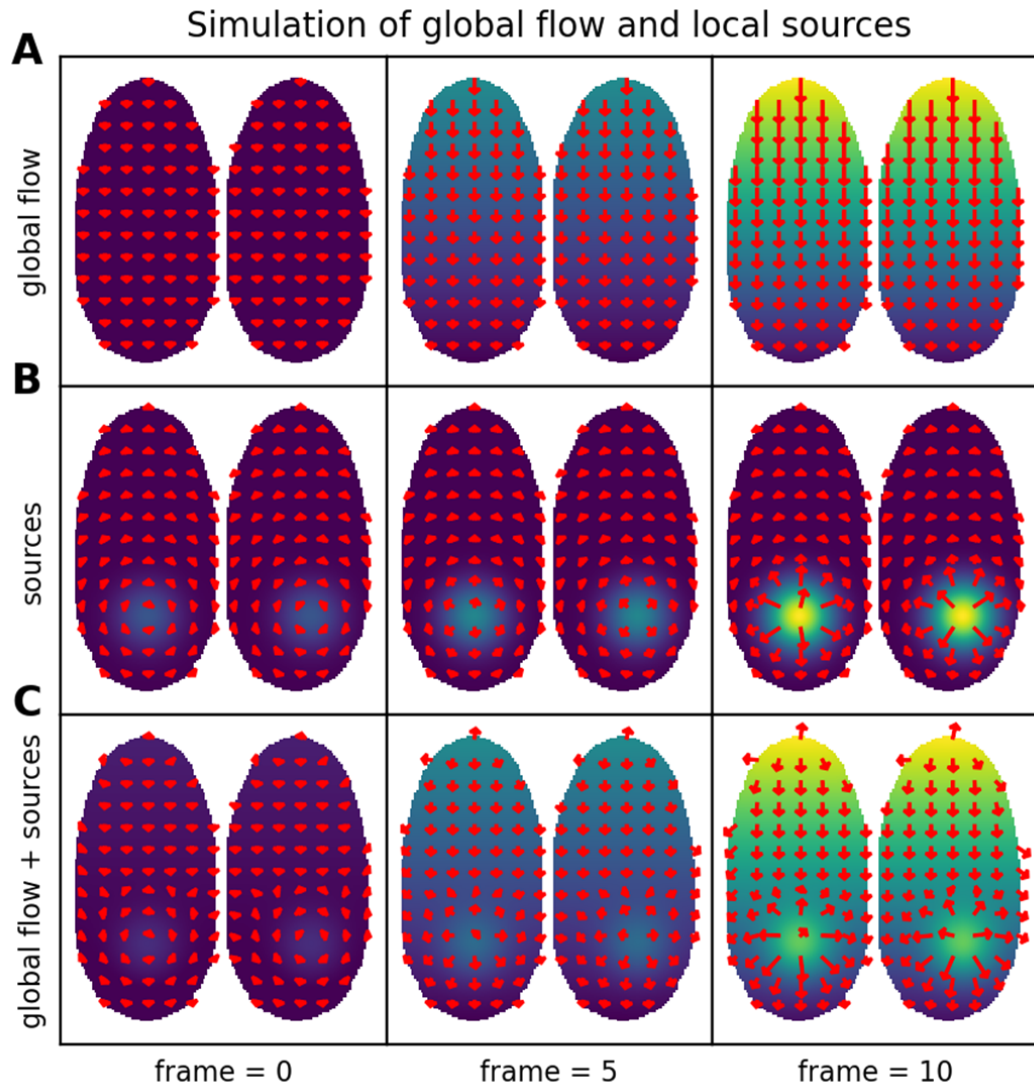


Figure 3.6: Optical flow for a simulated signal

Panel A (top row): Three frames from a sequence where a global brightness gradient increases in intensity. Panel B (middle row): Areas of focal brightness change and the resulting sources and sinks. Panel C (lower row): The sum of the signal in A and B. Optical flow was computed for each sequence of frames and is plotted in the foreground.

for each frame the three signals. The Optical Flow of the combined signal was then decomposed into the distribution of sources and sinks as well as the flow component.

It shows that the distribution of sources reflects focal areas of an increase in brightness. In the fluorescence recordings this local increase can be assumed to result from recurrent activity in distinct areas of the brain. In contrast the vector field of the flow component reflects the Optical Flow of the first of the three simulated signals. The impact of focal brightness changes on the vector

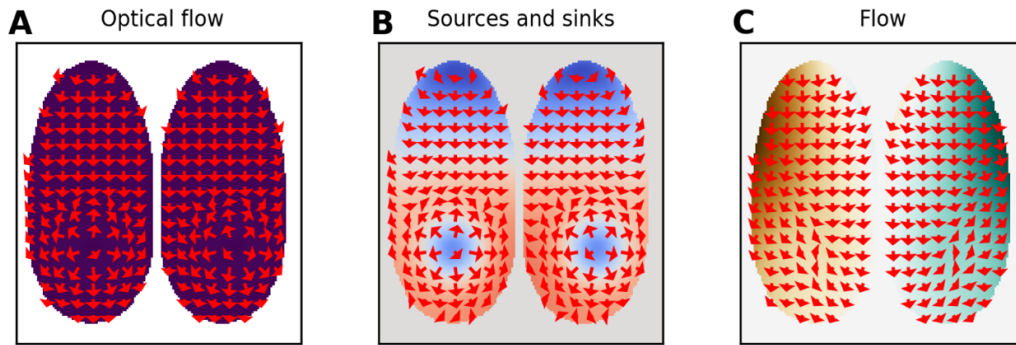


Figure 3.7: Helmholtz Decomposition of Optical Flow.

Panel A: A vector field of Dense Optical Flow that contains sources and global flow. The respective brightness distribution is shown in the background (see also Figure 3.6C). Panel B: The distribution of sources and sinks retrieved using Helmholtz Decomposition of the vector field in A. The scalar potential is plotted in the background. Note that focal areas of brightness increase have positive values in the scalar potential of the curl free component. Panel C: The flow component of the vector field in A. Note that the impact of focal areas of brightness increase on the resulting flow field is highly reduced. Helmholtz-Decomposition allows to distinguish global flow from focal areas of brightness increase or decrease.

fields can be highly reduced. The flow component can be assumed to reflect scenarios where peak activity shifts from one area to another or a global wave spreads through a hemisphere.

3.4 Autoencoders

Neuroimaging techniques allow for the acquisition of data with a high temporospatial resolution. This means that the recordings are of high dimensionality. However specific features are especially interesting: The location of focal areas of recurrent activity, the amplitude of the event and the direction of flow. Feature engineering that relies on Optical Flow and Autoencoders can be used to retrieve these features with a high degree of control. This allows to reduce the dimensionality of the data and promises robust features. Further dimension reduction can be achieved using unsupervised learning. It can be assumed that slow waves are either similar with respect to the mentioned properties or to differ substantially. Low dimensional representations can help to identify different types of slow waves. Here Autoencoders are used for dimensionality reduction as they allow for the approximation of non-linear functions and are well suited for images.

Autoencoders can be understood as a more general approach to dimension reduction as compared to Principal Component Analysis (PCA). An Autoencoder with a single hidden layer, a linear activation function and a squared error cost function is almost identical to PCA: After successful training the weights span the same subspace as the Eigenvectors in PCA. However, the weights are not necessarily identical (Plaut, 2018). Both PCA and single layer, linear Autoencoders with squared error loss can be used to linearly map data onto a lower dimensional subspace³. Simple Autoencoders employ a Multi-layer Perceptron (MLP) as the encoder and decoder. Here MLP is used in the strict sense and relates to feedforward networks that comprise of fully connected layers only. This form of Autoencoder was described as an alternative to PCA already when the computational power of available machines was limited (Kramer, 1991). In the most simple case weights are learned using gradient descent and backpropagation to minimize the reconstruction loss only: In this case the data is used as both the input layer activation and the output layer activation. MLPs are nonlinear function approximators and hence promise better reconstructions for low dimensional latent layers as compared to linear mappings. Autoencoders represent a powerful and flexible tool for the unsupervised analysis of high dimensional data.

There are numerous applications of Autoencoders in biomedical imaging and neuroscience for various domains of data. Autoencoders that employ convolutional layers are especially well-suited for images. For example Autoencoders can be used to detect tumors in the brain or the liver using Magnetic Resonance Imaging (MRI) or Computer Tomography (CT) (Mallick et al., 2019; Sital et al., 2020). Similarly they can be used to label and detect brain lesions (Alex et al., 2017). Autoencoders can also be used in combination with fMRI. For example it was shown that the visual perception of participants can be decoded from fMRI recordings. A variational Autoencoder (VAE) is trained on the videos that participants watched during data acquisition and a linear regression model mapping is used to map the BOLD response to the latent layer activations such that the decoder can predict the frames (Han et al., 2019). Autoencoders can be used for unsupervised learning and semi-supervised learning. The latter case is especially relevant if labels exist for a subset of the dataset. Besides there are several ways in

³Here it is assumed the Autoencoder has fewer latent layer neurons than inputs. Note that Autoencoders could in principle also have latent layers with a higher dimensionality as the input and target layers. A typical example are sparse Autoencoders (PapersWithCode, 2021b).

which Autoencoders can be used aiming for potentially different objectives. Multiple examples exist:

- (1) Dimension reduction. If Autoencoders are used for dimension reduction the latent layer activation is of interest. The same data that is used for the input layer is predicted by the output layer (Han et al., 2019).
- (2) Artifact removal and denoising. If Autoencoders are used for artifact removal or denoising data with artifacts is used as the input to predict an artifact free version. Denoising Autoencoders are models that are trained on data with added noise to avoid learning the identity function which is especially important if the bottleneck layers are of high dimensionality (PapersWithCode, 2021a)
- (3) Attribution of pixelwise labels. In this case source data is used which is different from the target data. A common example is semantic labelling of natural images or medical images. In this case semi-supervised learning is employed (Alex et al., 2017).
- (4) Domain transfer. An example for domain transfer is the mapping between 2D images and 3D point clouds (Lin, Kong, and Lucey, 2018).
- (5) Semantic Image Augmentation. An example for this category is image colorization (Anwar et al., 2020).

Different versions of Autoencoders exist that employ a custom loss function. Besides modifications that are necessary to achieve good predictions there are loss functions that are used to shape latent space. The most well-known examples are VAEs and Autoencoders for semisupervised learning. Here VAEs are used. The loss function of a VAE contains the reconstruction loss which is added to a second term (the KL-loss), that is based on the Kullback–Leibler divergence and penalizes noncontinuous distributions of the data in latent space. The models used here were derived from standard VAEs. The activation of the latent layer z depends on the resampled activity of two previous layers z_{mean} and z_{logvar} that connect it to the encoder and have a linear activation function. The resampling function is given by Equation 3.8. The KL-loss is given by Equation 3.9.

$$\text{sampling}(Z_{mean}, Z_{logvar}) = Z_{mean} + \exp(0.5 * Z_{logvar}) * \mathcal{N}(\mu = 0, \sigma^2 = 1) \quad (3.8)$$

$$\text{KL}_{loss} = -0.5 * \sum 1 + Z_{logvar} - Z_{mean}^2 - \exp(Z_{logvar}) \quad (3.9)$$

The structure of Autoencoders depends on the objective for which they are used and has to meet the constraints of the data. Deep Autoencoders that employ strategies to overcome the vanishing gradient problem have been employed with great success to label medical data (Du et al., 2020). An example is UNet which uses direct links that connect early layers of the encoder and late layers of the decoder. In the moste simple version (Base UNet) links are achieved by concatenation of the output from the contracting path to inputs of layers of the expansive path. In other variations such as UNet++, additional convolutional layers are used between encoder and decoder (Du et al., 2020). UNet can also be used as part of a generative adversarial network. In this case a discriminator network is connected to the output of the decoder to distinguish between generated labels and training labels. Generative adversarial networks promise reconstructions with higher levels of detail. Variations of UNet have been used for tissue segmentation and cancer detection in numerous studies using MRT, MRI and ultrasound (Du et al., 2020).

Here Autoencoders are used on relatively sparse features as only specific properties of the data are of interest and major parts of the variance are arguably not necessary to reflect them. The main purpose is dimension reduction. The possibility to assess the quality of intermediate representations and to compute meaningful aggregations could help increasing the interpretability of the results. Training on sparse features also means that comparatatively shallow networks can be used.

Three different Autoencoders were implemented to analyse the extracted slow wave features. The first Autoencoder was used to analyse the distribution of the detected samples in slow-wave-shape-space. It showed that different events have similar signatures in the df/f signal. Hence it was aimed for a simple Autoencoder that can be used to encode relatively sparse values. A simple MLP-Autoencoder was implemented for this purpose where all layers are fully connected. As different slow waves were found to have

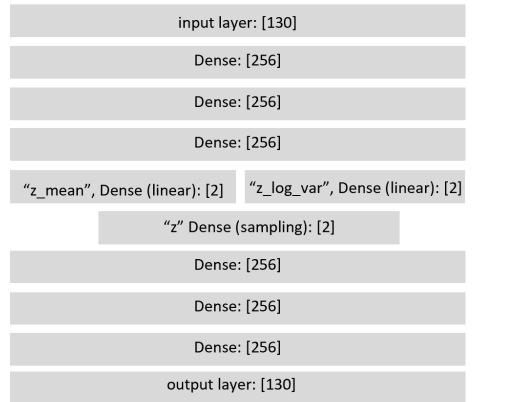


Figure 3.8: Structure of the MLP-Autoencoder.

This Autoencoder was used for the analysis of slow-wave-shape space. Rectified linear units (RELU) activation functions were used if not stated otherwise. The df/f signals for each detected event are normalized and interpolated to be of equal length (128 entries). The duration and amplitude of each event were appended.

similar shapes but differ in amplitude the df/f signal of each event was normalized and interpolated and the peak amplitude was appended. This approach was chosen such that it is possible to exert control over the impact of differences in amplitude on the reconstruction loss. The resulting structure of latent space reflects similarities in shape and size of events.

The second Autoencoder represents a mixed input model (Figure 3.9). Several different features were used as the input and output activations. These features include grayscale images that represent the mean distribution of sources and sinks for each event, the normalized df/f signal, the phase and peak amplitude as well as the ratio between upwards, downwards leftwards and rightwards flow. Different modules were implemented for the encoder and decoder that were considered best suited for the respective type of data. Images and time series represent data that contains local features. Hence 2D convolution was used for the distribution of sources and sinks. In contrast 1D convolution was used for the time series. 1D convolution was realized using 2D convolution with 1XN shaped kernels. MLP layers were used for the scalar values.

$$\text{loss} = \text{KL}_{\text{loss}}(z_{\text{mean}}, z_{\log\text{var}}) + \sum p_i * \text{MSE}(\text{data}_i, \text{VAE}(\text{data})_i) \quad (3.10)$$

$$\text{MSE} = \frac{1}{n} \sum_{i=0}^n (x_i - y_i)^2 \quad (3.11)$$

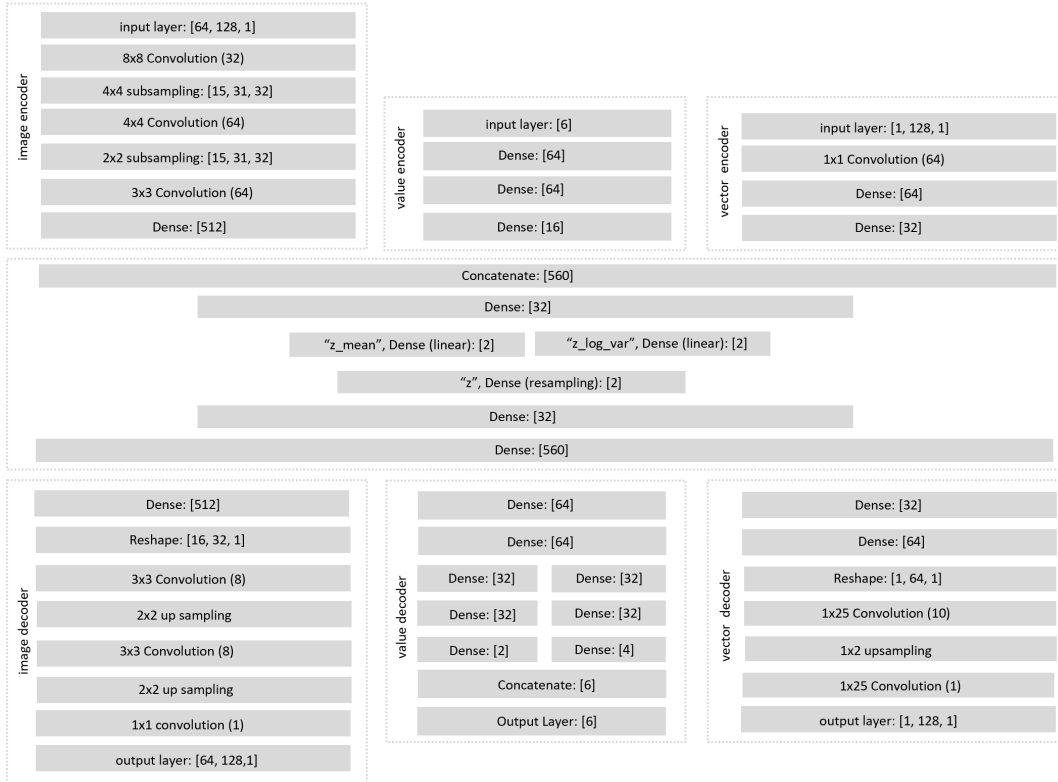


Figure 3.9: Structure of the mixed input Autoencoder.

This Autoencoder was used to analyze (1) the distribution of sources and sinks (2) the df/f signal and (3) scalar values that reflect the amount of flow in upwards, downwards rightwards and leftwards direction alongside the duration and amplitude of each event. Different encoders and decoders were used for each domain of data. 2D convolution was used for encoding and decoding the distribution of sources and sinks, 1D convolution was used for the time series signal and fully connected MLP layers for the scalars. Note that different branches were introduced in the respective value decoder. This was found to help optimizing the predictions for the directions of flow and at the same time the duration and amplitude of each event. RELU activation functions were used if not stated otherwise.

A custom loss function was used to ensure that all of the encoded features are well reflected in the reconstructions. The respective function is given by Equation 3.10 where MSE relates to the mean squared error, data is a set of the image input, the time series input, as well as the input for duration and amplitude and the input for the ratio of flow in upwards, downwards, leftwards and rightwards direction. Here, VAE stands for the variational Autoencoder depicted in Figure 3.9. The weights p_i for the individual terms in the loss functions were adjusted manually while changes to the network structure were made until the predictions correlated strongly with the data. This was assessed by correlation in the case of the sparse features (duration, amplitude and the ratio of flow) and qualitatively in the case of images and time series.

The third Autoencoder is an example that employs multiple 1D convolution.

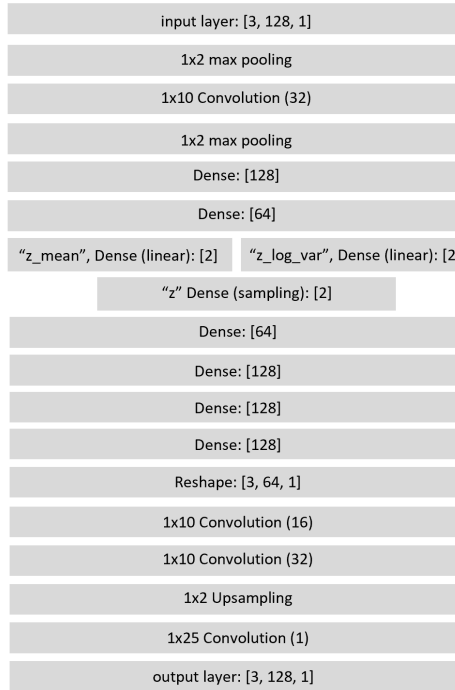


Figure 3.10: Structure of the Autoencoder for time series analysis.
This model was used for the analysis of the df/f signal and the upwards and downwards flow. Note that multiple 1D convolution is achieved using 2D convolution with kernels of shape 1xN. RELU activation functions were used if not stated otherwise.

1D convolution was again realized using 1xN kernels in 2D convolutional layers. It was used to meet the local nature of time series data. Several layers are employed to form a deep network. In addition, multiple fully connected layers are used to connect named convolutional layers to the input and output layer respectively. The choice of kernel sizes has proven to be crucial for the network performance.

All three networks use a variational loss that includes the KL-loss and a term that penalizes poor reconstructions. The mean squared error is used as a metric for the quality of the decodings. No distinctions were made for different types of data. The reconstruction loss was weighted with $p_0 = 10$ in the case of the first model and $p_0 = 100$ for the last one. In the mixed input Autoencoder a separate reconstruction loss was used for each of the three encoder decoder pairs. The weights are $p_0 = 1$ (for the images), $p_1 = 20$ (for the time series) $p_2 = 32$ (for the amplitude and duration) and $p_3 = 16$ (for the ratio of flow in different directions).

3.5 The processing pipeline

Several processing steps were employed to retrieve a contrast that is suitable for the application of Optical Flow and reflects the activity neocortical slow waves. Figure 3.11 gives an account of the approach while Figure 3.12 illustrates the processing pipeline in greater detail. In the first stage the df/f normalized signal change was computed for each recording (Figure 3.12: Preprocessing). This signal was integrated spatially to compute the mean signal in time and used to detect slow wave events in the second stage (Figure 3.12: Segmentation). An improved contrast was computed in the third stage for each of the detected periods separately (Figure 3.12: Postprocessing).

Widefield fluorescence microscopy makes use of selective differences in the reflectance of light of a specific wavelength that results from conformational changes of ion channels in the neural membrane. The approach is challenged by the hemodynamic autofluorescence due to fluctuations in the blood oxygen level. The fluorescence of oxygenated and deoxygenated hemoglobin depends on the frequency of the light used for illumination. At a wavelength of 405nm the differences are marginal (Figure 3.11:A). Hence the respective signal is referred to as GCaMP signal here. Nonetheless a hemodynamic error signal remains in the data. As it was found that high frequency oscillations relate to the bloodflow band stop filtering and smoothing were employed in preprocessing to reduce the effect of hemodynamics. The degree of temporal smoothing must be limited as fast spreading signals can otherwise not be detected. Components in the bandstop filtered signal that correspond to the heartbeat are absent in the result.

To assess the relationship between the GCaMP signal and the hemodynamic signal a second video was simultaneously recorded at 460nm using polarization filters and beamsplitters (Figure 3.11:A). This hemodynamic signal was preprocessed in the same way as the GCaMP signal. High frequencies that include the range of the heartbeat are removed. It shows, that oscillations which are correlated to breathing are present in the signal. Removing this effect has proven difficult on the level of individual pixels especially considering the requirement of a high temporal resolution that prohibits strong temporal smoothing. There is evidence which indicates that low amplitude oscillations in the GCaMP signal could at least partially include neural effects.

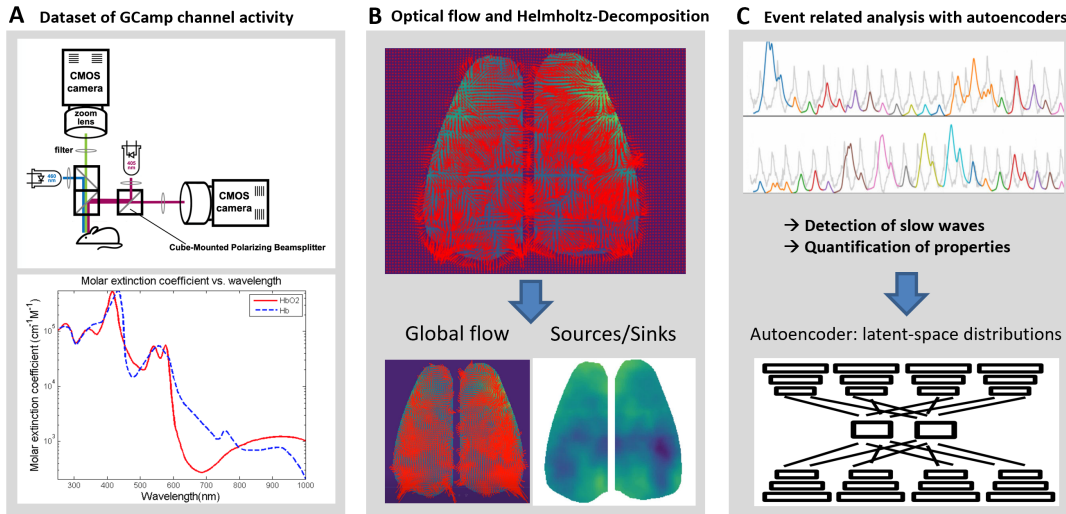


Figure 3.11: Outline of the approach

Panel A: Dataset of GCamp channel activity. The main dataset used to develop and evaluate the approach presented here includes recordings of GCamp fluorescence of transgenic mice. Recordings were acquired for different stages of anaesthesia ranging from 1.8% isoflurane to 2.6%. The sampling rate is 100Hz with a spatial resolution of 300x260px. GCamp fluorescence was recorded under illumination with light at 460nm. The hemodynamic fluorescence was recorded at 25Hz under illumination with light of 405nm wavelength. Polarization filters and beam splitters were used to acquire both signals at the same time. All depictions of Panel A were provided by Westmeyer Laboratory. All recordings were performed by Silviu Bodea at Westmeyer Laboratory at Technische Universität München. Panel B: Optical Flow and Helmholtz-Decompositon. The panel shows schematically how optical-flow can be estimated and decomposed into a global flow-field and a distribution of sources and sinks. This allows for the evaluation of pathways of neural signal transduction alongside the analysis of the spatial distribution of sources and sinks. Note that important features are derived from Optical Flow and Helmholtz-Decomposition but additional properties such as the correlation with the hemodynamic signal can be included in the analysis as well. Panel C: Event related analysis with autoencoders. The mean percentage change of the signal in time is used to identify individual slow-waves in a scale independent manner. This allows for the quantification of properties per-wave in an event-related design. Autoencoders are used to identify the relationship between properties of slow-waves including the experimental condition they stem from and aggregations of the results of Helmholtz Decomposition.

Arguments for respiration coupled neural effects can be summarized as follows. First the location of peak activity in the GCaMP signal and the hemodynamic signal can deviate. There is little coherence between the spatial distribution of both signals at peak activity. Second respiration coupled slow waves are not always perfectly phase locked with the hemodynamic signals but there can be a varying offset between the respiratory peaks in the GCaMP and the hemodynamic signal. While the amplitude of slow oscillations in the

mean hemodynamic signal is relatively constant, the corresponding oscillations in the mean GCaMP signal can vary substantially - especially during deep anaesthesia. A possible explanation is that breathing coupled neural activity elicits neocortical slow waves in some cases while it is not sufficient in others. Finally, respiration coupled oscillations can be recorded using ECoG and have recently been proposed to represent an independant brain rythm that affects cortex (Tort et al., 2018). As the question regarding the origin of breathing coupled oscillations in the GCaMP signal could not be finally answered no further efforts were taken towards a removal.

Slow waves are understood as extended periods of neural firing. ECoG data shows that several oscillations can occur during each event. The preprocessed df/f signal was further baseline corrected and used to distinguish events based on local minima. The minimal convex hull can be used for baseline correction. The df/f signal is (1) added to a parabola, (2) the convex hull is computed ("rubberband fit") and (3) subtracted from the signal. Because it is assumed that slow waves can include several oscillations events are not split at every local minimum. Instead a scanning procedure was implemented to determine local minima that define the start and stop positions. Beginning with the time of the first local minimum as start, subsequent local minima are evaluated recursively and defined as the stop of the current event if the activity is sufficiently close to baseline. The latter condition holds if the value $f(\text{stop})$ is not larger than $f(\text{start}) + \epsilon$. Epsilon is expressed as the current height of the event i.e. the absolute difference between $f(\text{start})$ and the maximal value between $f(\text{start})$ and $f(\text{stop})$. The approach allows to split events of different magnitude without using a hard threshold.

The indices that result from the splitting procedure are used to compute a contrast for each event seperately. The computation of the df/f signal per event has two advantages. First movements of the animal do not affect the whole contrast for the whole recording. If the animal moves slightly the mean image and the individual frames are misaligned. This leads to artifacts in the df/f signal. In an event related design this affects at worst single events. Similarly it allows to subtract the mean image after computing the background to improve the contrast as suggested by Celotto et al. (Celotto et al., 2020). Second the mean image represents a biased proxy for an image of the brain where no GCaMP flourescence occurs. In average slow wave activity is stronger in certain regions, hence the mean image is brighter. While

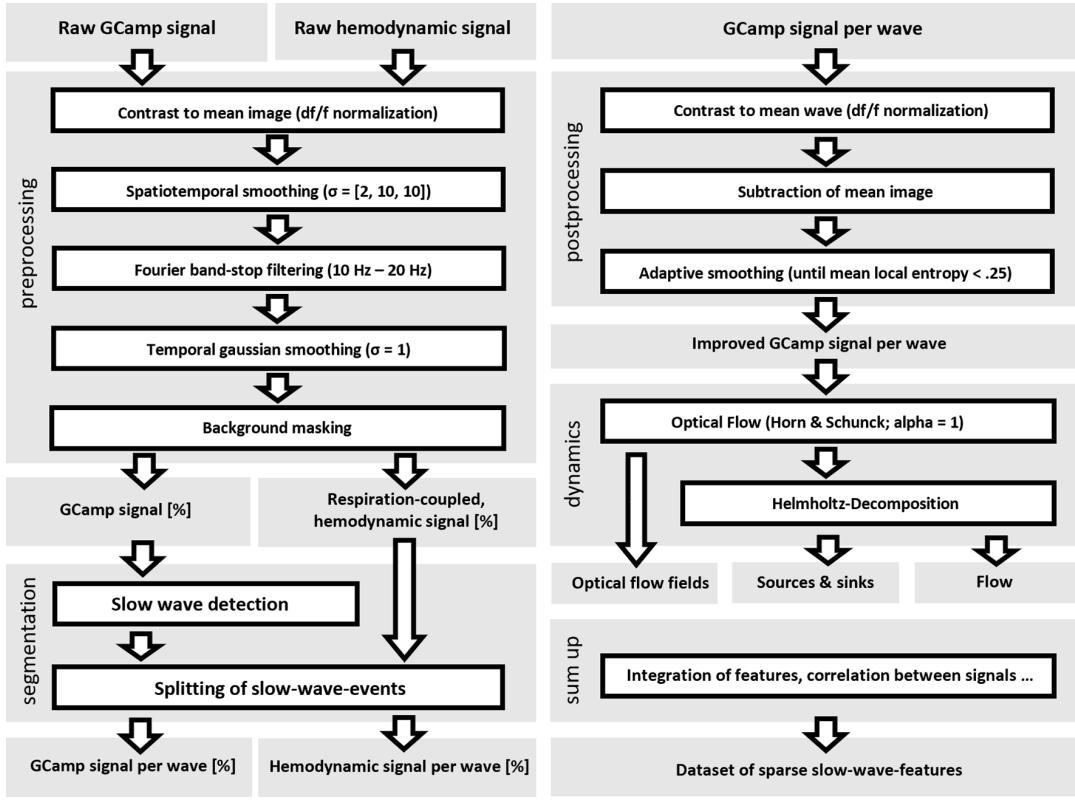


Figure 3.12: The processing pipeline

this does not impose a problem for large amplitude events it is clearly visible as a spatial bias in the df/f signal of small amplitude events. If the contrast is computed for each event separately this effect is reduced and local differences become visible.

In the last two steps of the pipeline Optical Flow and Helmholtz Decomposition are used to characterize the dynamics of the events and several features are aggregated and stored in a sparse dataset. This dataset contains information about the df/f signal, the distribution of sources and sinks as well as several aggregations of the vector fields of the flow component.

Chapter 4

Results

4.1 Qualitative and quantitative descriptions of slow waves

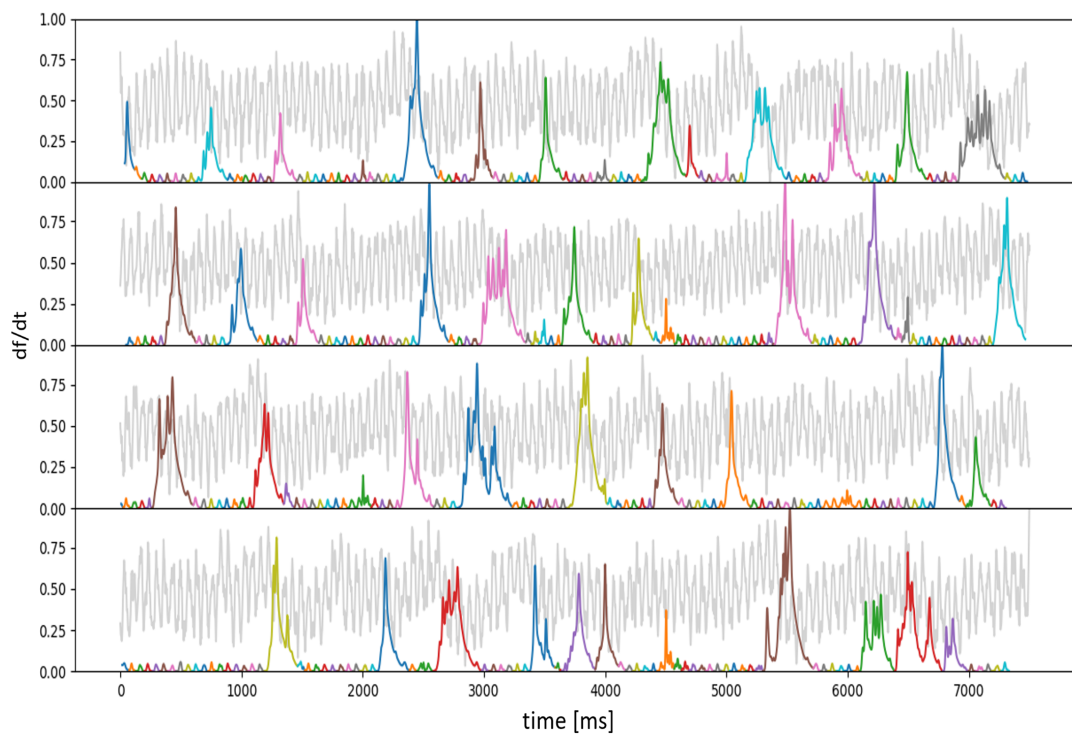


Figure 4.1: Detected slow waves for a sample recording at 1.8 % isoflurane. The depiction shows the results of the splitting procedure. Segments of the baseline-corrected mean percentage change that were identified as one event are represented in the same color. Note that the approach identifies events in a scale independent manner. Colors indicate segments of the df/f signal for a complete recording (GCaMP). The hemodynamic signal is plotted in grey.

The approach for the analysis of slow waves includes three steps: Detection of events, feature extraction using Optical Flow and Helmholtz-Decompositon as well as dimension reduction by aggregation and the use of Autoencoders. Slow oscillations were detected in the df/f signal such that an event related

analysis could be performed. Aggregated features were analyzed quantitatively. Moreover individual waves were investigated qualitatively in more detail. This analysis includes several features such as the peak amplitudes and the directions of flow on one side as well as the vector fields on the other. The results are presented in this section.

Figure 4.1 shows an example for the detection of slow waves for a sample

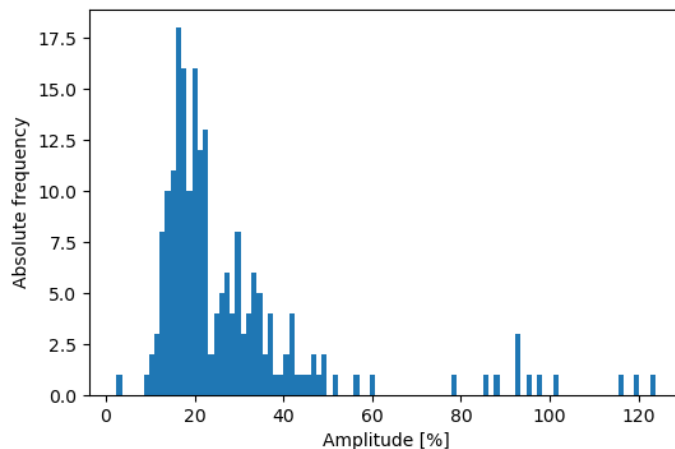


Figure 4.2: Distribution of the peak amplitude of detected waves.
The depiction shows the distribution of the peak amplitude of the selected slow waves after cleaning the dataset. Cleaning includes removal of instances that are highly correlated ($r>.3$) with the hemodynamic breathing signal. In addition, it comprises the removal of waves for which the peak activity of the mean percentage change in time is less than 5% of the duration. Note that events with a peak amplitude of below 5% are virtually absent.

recording ($\text{iso} = 1.8\%$). The procedure was found to yield segmentations that meet the human intuition for all stages of anaesthesia. Note that several of the depicted events are similar with respect to shape and size. Different types can be distinguished. Some events have a single peak while others have multiple ones and show longer up states.

Note that a trend in the hemodynamic signal is related to the occurrence of large amplitude events: While the hemodynamic signal appears to increase before the occurrence of large amplitude events it drops during the respective neocortical slow wave. The latter arguably indicates effects of neurometabolic coupling and represents a BOLD response. The circumstance that a rise in the hemodynamic signal precedes neocortical slow waves could mean that higher blood oxygen levels promote the occurrence of runaway neural firing.

Events for which the df/f signal correlates strongly with the hemodynamic

signal were excluded from the further analysis. These events relate to large amplitude neocortical slow waves that have a good signal to noise ratio. It was found that the most interesting patterns are visible for these events. Waves with a peak amplitude below 5% are virtually absent in the filtered dataset of slow waves. The dataset of large amplitude slow waves includes 204 samples from two animals and five experimental conditions. Figure 4.2 shows the distribution of peak amplitudes.

The activity of neurons is inhibited at higher dosages of isoflurane (Figure 4.3: B). This results in widespread quiescence for deep anaesthesia. Coherently it shows that the distribution of slow wave amplitudes decreases for higher levels of isoflurane. While neocortical slow waves occur with a peak amplitude of up to 120% signal change they mostly rely around 20 % for an isoflurane level of 2.6%.

The shape of the events differs between conditions. Typical examples of

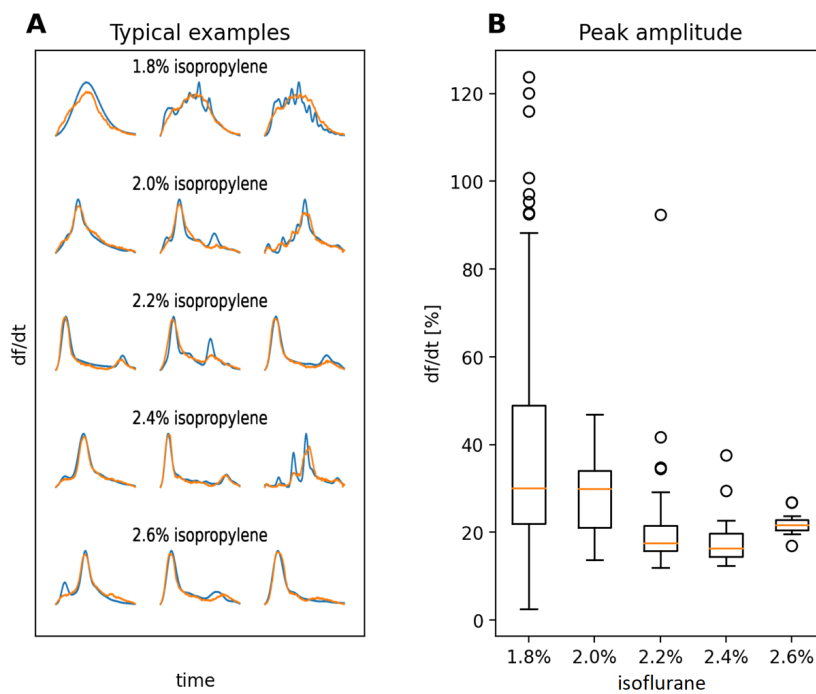


Figure 4.3: Typical examples and peak amplitudes.
The depiction shows data for slow waves with a peak amplitude above 5% that are only weakly correlated with the hemodynamic signal ($r < .3$). Panel A: Typical examples for slow-wave events during different stages of anesthesia. The mean signal change over time is indicated in blue while reconstructions of the Variational Autoencoder with fully connected layers are plotted in orange. Panel B: The distribution of the peak amplitudes of the mean signal over time for each slow wave per condition.

the df/f signal and the reconstructions of the Autoencoder for the slow wave

shape space are indicated by Figure 4.3:A. At 1.8% isoflurane slow waves are present that have an extended up state and multiple peaks. Single peak waves and waves with two larger peaks are especially characteristic for 1.8% and 2.0% isoflurane. At higher levels of anesthesia another type can be observed that comprises of one major peak and a much smaller one that occurs subsequently. This type of neocortical slow wave arguably reflects synchrony between neural firing and breathing (see also Tort et al., 2018). Its shape results from a major neocortical slow wave that is followed by a peak which is correlated with the breathing signal. While different types of neocortical slow waves occur preferably for specific concentrations of isoflurane each condition can be described as a composition of different types of events.

A general distinction of the spread of neural signals can be made for bottom

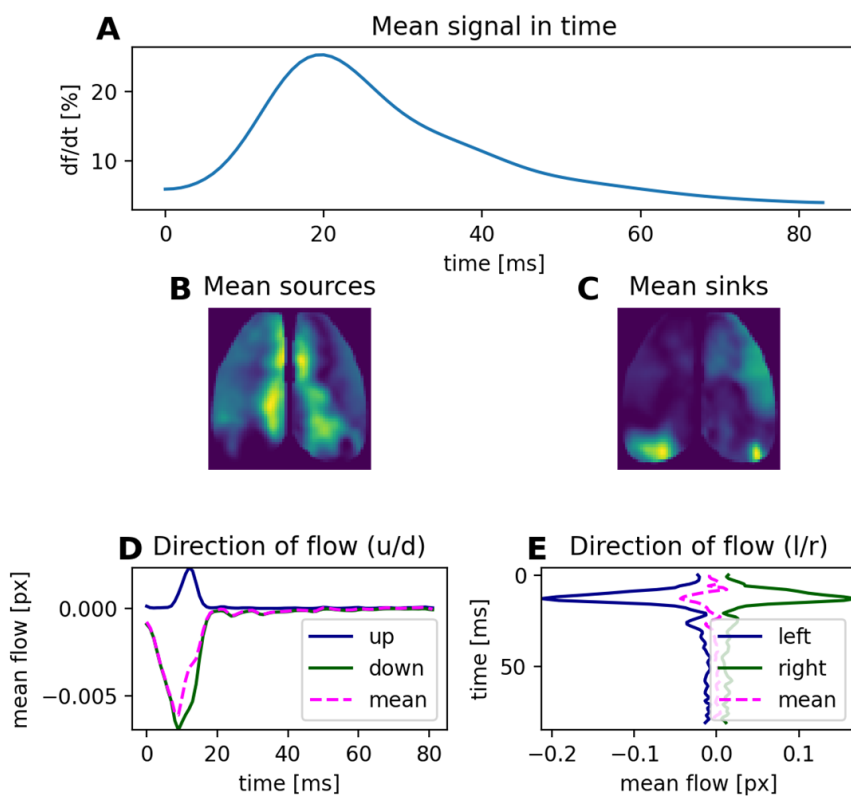


Figure 4.4: A typical example with one peak.

Percentage change, direction of flow and the distribution of sources and sinks. Panel A shows the mean percentage change in time. Panel B illustrates the mean sources and sinks distribution in space and Panel C illustrates the mean sinks distribution respectively. Note that the brain regions that act as sources are not identical with the regions that act as sinks which supports the idea of a sender-receiver pattern. Panels D and E indicate the direction of flow in vertical direction (up/down) and horizontal direction (leftwards/rightwards) respectively.

up and top down flow. In the mouse cortex, bottom up flow can originate from auditory and visual areas in the occipital lobe as well as retrosplenial dysgranular cortex (RSD) which contains neural populations that code for places and is thought to integrate thalamic, hippocampal, and neocortical information (Milczarek, Vann, and Sengpiel, 2018; Groen and Wyss, 1992). It shows that there is a trend towards lower levels of bottom up flow for higher levels of isoflurane. However this trend is not significant (see Figure 4.5).

The vector fields of the flow component can be evaluated qualitatively. Fig-

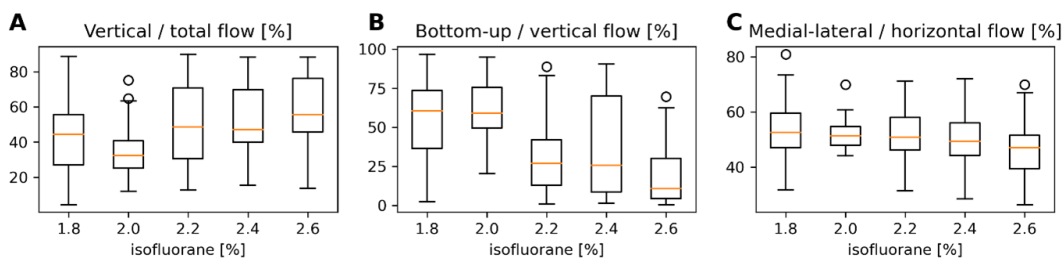


Figure 4.5: The direction of flow for different levels of isoflurane.

Panel A: Vertical flow (the sum of the absolute Y-components of the vectors of the flow field) as a proportion of total flow. Panel B: Bottom-up flow as a proportion of vertical flow. Panel C: Medial to lateral flow as a proportion of horizontal flow (the sum of absolute X-components of the vectors of the flow field). Note that the flow component retrieved via Helmholtz-Decomposition of the Optical-Flow are the basis for the aggregated data displayed here.

ure 4.6 illustrates the relationship between the df/f signal, the field strength and the vector field of flow for an example with a single peak where downwards and leftwards flow can be observed in the left hemisphere. In the right hemisphere mainly right-downwards flow occurs. However, at peak activity rightwards flow dominates. The dynamics of the event are also illustrated by Figure 4.4. The aggregations reflect the flow of the left hemisphere. Here the distribution of sources and sinks is plotted as well. Areas on the medial axis act as the main sources while visual areas act as sinks. The direction of flow and the distribution of sources and sinks characterize neocortical slow waves.

It is to mention that the spatial distribution of sources does not directly compare with the mean activity in space as measured by the df/f signal of an event. The temporal integral of the df/f signal does not reflect the distribution of sources as sources indicate focal areas of brightness increase. While the mean across all frames of the df/f signal can show little spatial variations the mean of the sources distributions reveals focal area of increasing neural

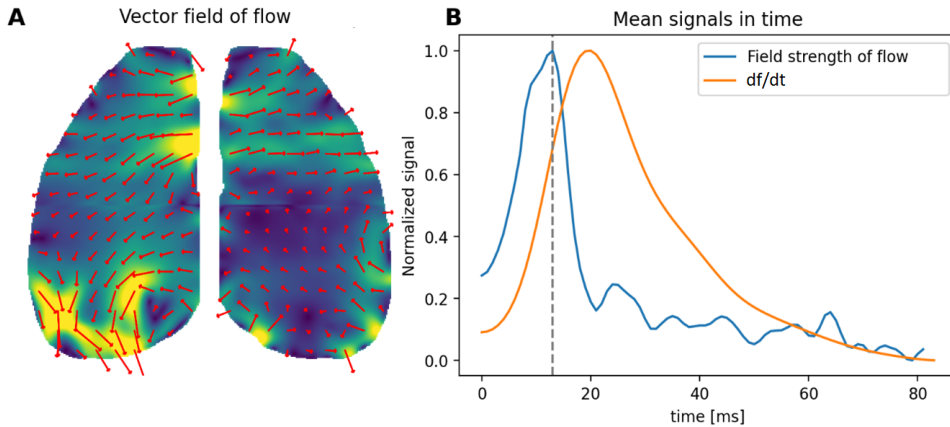


Figure 4.6: A sample vector field and field strength of flow in time.
The depiction shows a vector field for a slow-wave event at 1.8% isoflurane alongside the mean percentage change and mean flow in time. Panel A: The vector field representation of the flow component. The field strength is plotted in the background. Panel B: The mean percentage change in time and the mean field strength of the flow component. Note that the signals are not to scale. The time of the depicted frame is marked by a vertical dotted line. Left-downwards flow shows for the left hemisphere.

activity (Figure 4.7).

Neocortical slow waves can incorporate several oscillations (see section 2.6).

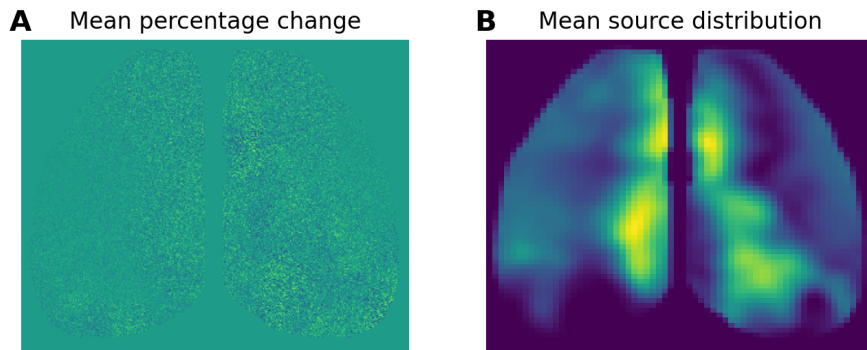


Figure 4.7: The temporal mean of the df/f signal and the sources.
The depiction illustrates that the temporal mean over all frames showing the df/f signal is highly dissimilar from the temporal mean of the sources for the same period. This shows the benefits of Helmholtz Decomposition applied on Dense Optical Flow. The approach allows to reduce dynamical changes of neural activity that occur during slow waves to a lower dimensional representation that reflects functionally connected regions.

In addition it can be assumed that even events with a single peak can incorporate several subsegments for which different areas act as sources or sinks and different patterns occur in the flow. To test this assumption slow waves were split into subsegments based on the local minima in the distribution of

the sources. Figure 4.8 illustrates the results. During different stages of the slow wave distinct areas represent the sources. It shows that this distribution can be distinguished into a lateral cluster that includes somatosensory areas (e.g. segment onset at 21ms) and a medial cluster that includes regions on the medial axis from frontal to occipital cortex (e.g. the last segment). These findings represent first evidence that different stages of slow waves exist in events that show only one peak in the temporal mean of the df/f signal. As the strength of sources during downstream periods is weaker they are however more prone to artifacts in the contrast (see also 3.5). More research is required to systematically study the events that occur during different stages of neocortical slow waves.

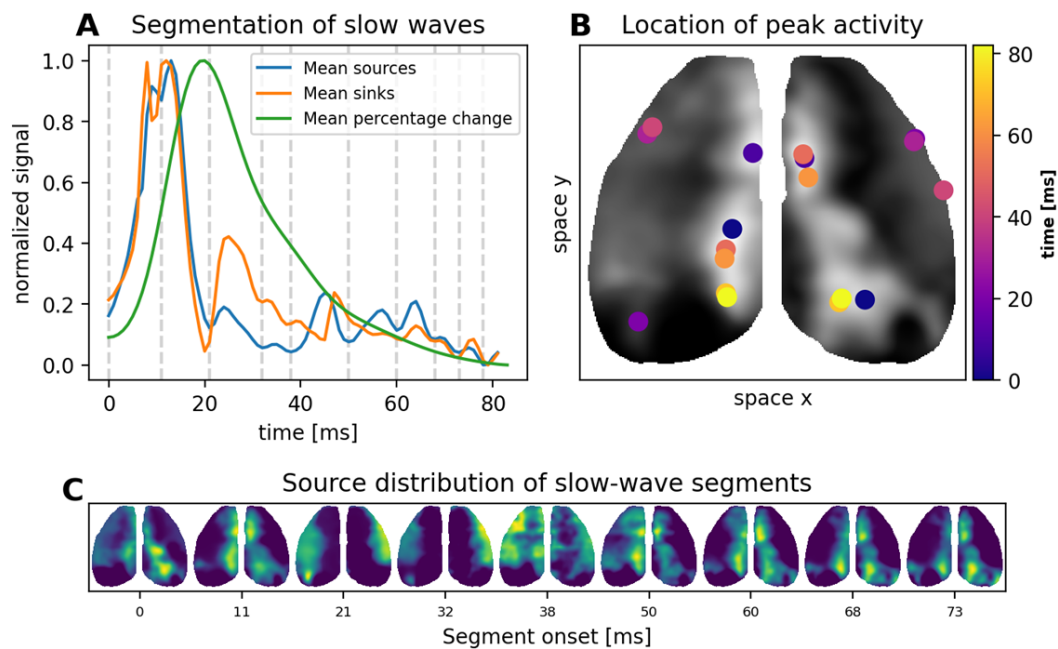


Figure 4.8: Slow wave subsegments.

The depiction illustrates the procedure of splitting a slow wave into subsegments using the mean sources distribution. Panel A: The mean signal in time for the sources and sinks alongside the mean percentage change. Slow-wave segments are determined using local minima in the mean sources signal in time. Gray dotted lines indicate the onset and offset of each segment. Panel B: The location of peak activity. Panel B shows the location of maximal activity for the mean source signal in space of each subsegment (see Panel C). Note that the time of segment-onset is indicated by different colours. Each dot corresponds to the segments identified in A and the mean source signal in space in C. Panel C: The temporal mean of the source signal in space for the identified slow-wave segments. Note that the depictions normalized before a colormap was applied to increase the contrast. Yellow tones relate to higher values.

4.2 Reconstruction manifolds and latent space distributions

Several different types of neocortical slow waves can be discerned Intuitively based on the shape of the temporal mean of the respective df/f signal. Moreover the direction of flow and the distribution of sources differs between events. Besides it was argued that different compositions of events are characteristic for specific levels of anaesthesia. Autoencoders can be used for dimension reduction and represent a tool that allows to visualize the complex dynamics of slow wave anaesthesia. Three models were implemented. In the following the results of these models are presented that indicate (1) the distribution of several features in latent space and (2) can be used to compute manifolds of reconstructions. Autoencoders can help in revealing the complex dynamic of slow waves.

The first Autoencoder is a simple model that employs a MLP as encoder and decoder. As the input vector has few entries, fully connected layers can be used without compromising on the computational cost. The model reveals the distribution of several features in slow wave shape space. For the analysis presented here the Autoencoder was trained on the df/f signal for each event. Then the whole dataset was mapped onto the latent space. This space is spanned by the activation of the latent layer neurons $z[0]$ and $z[1]$. Several properties of each event can be visualized. Distinct regions in the low dimensional representation of neocortical slow waves relate to different types of waves. As a variational Autoencoder was used the latent space is comparatively densely populated. This means one may interpolate between events. Activations of the latent layer neurons can be chosen from an evenly spaced grid such that most of the data is covered. Using the decoder model the respective reconstructions can be retrieved. Figure 4.9 indicates this manifold alongside the distribution of several properties in latent slow wave shape space.

In general larger waves are mapped to the center while smaller waves rely in the periphery: The phase and amplitude is higher for the respective samples (4.9:F-G). The samples in the center region also have stronger flow as measured by the area under the df/f curve. Samples from the different experimental conditions are unevenly distributed in latent slow wave shape space. Most samples at an isoflurane level of 1.8% rely within the center and represent events with multiple peaks and extend upstate periods. At 2%

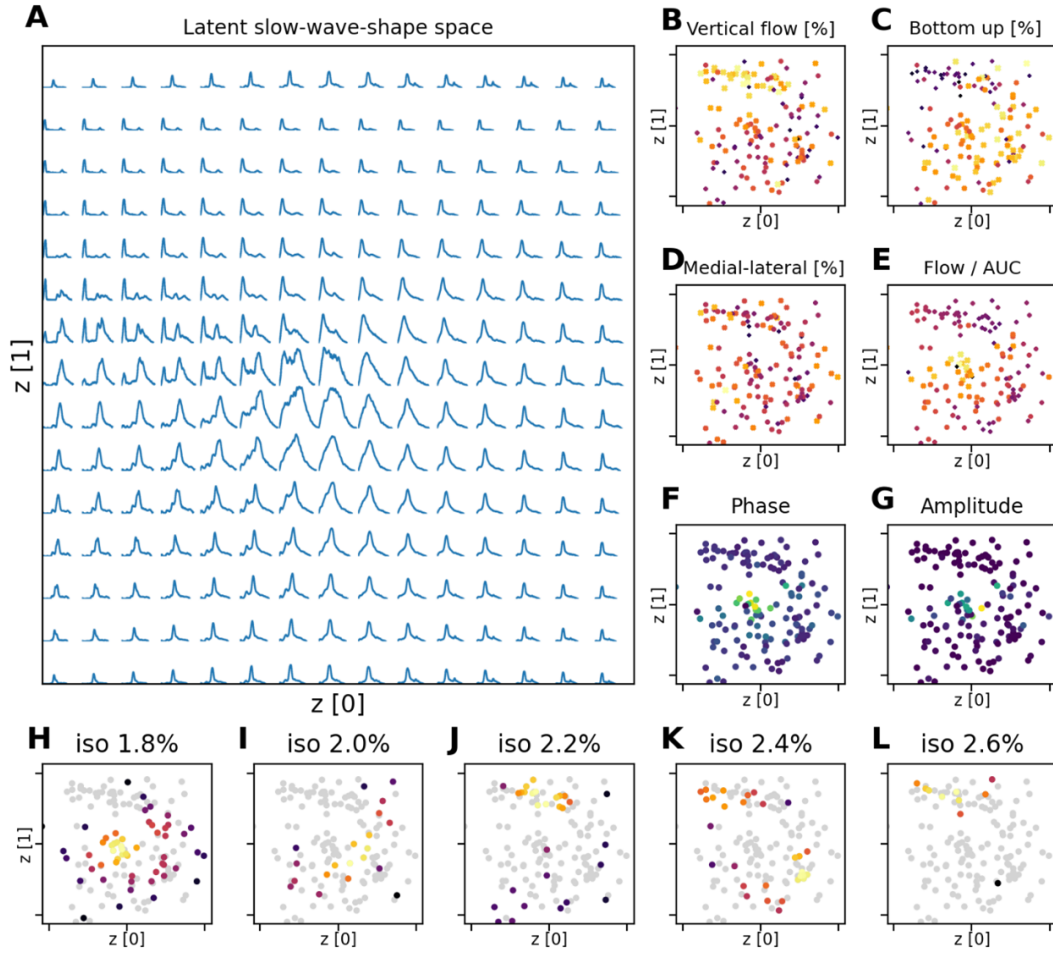


Figure 4.9: Latent slow wave shape space.

Note that events with peak-amplitude below 5% signal change and a high correlation with the hemodynamic breathing signal ($r > .3$) were excluded from the analysis. Panel A: Latent slow wave shape space. The panel shows a manifold of decodings for different combinations of the activation of the latent-layer neurons $z[0]$ and $z[1]$. Note that the latent-layer activations are chosen from an evenly spaced grid. The minimal and maximal values for each dimension of this grid are chosen as $\bar{z} \pm \delta(z)$ with $z = \text{encoder}(x)$. The decodings of the vectors are scaled according to the predictions of the width and height and plotted using a square root scale to ensure good visibility of small magnitude events. Panel B: The proportion of the absolute vertical flow as a fraction of the absolute flow during each wave. Panel C: The proportion of bottom-up flow as a fraction of the vertical flow. Panel D: The fraction of medial-lateral flow as a fraction of horizontal flow. Panel E: The ratio between mean absolute flow and the area under the curve of the mean percentage change for each wave. Panel F: The phase/duration of each event. Panel G: The distribution of the amplitude (peak of mean percentage change) for each of the events. Panels H-L: The distribution of samples in latent slow wave shape space.

more samples rely further to the lower right. These areas correspond to reconstructions that mainly represent neocortical slow waves with one major peak. For higher levels of isoflurane a cluster exists in the upper right. This

cluster arguably corresponds to waves where the smaller peak corresponds to an oscillation that is synchronous with the breathing signal. These samples have stronger vertical flow (as compared to horizontal flow) and less bottom-up flow as compared to top-down flow (4.9:B-D). Other samples of the very deep anaesthesia conditions ($\text{iso}>2\%$) are mapped to the periphery close to the lower and right border of the displayed subspace. This indicates a general shift from longer lasting up states with more oscillations to less dynamical states where smaller waves typically have only one peak.

The second Autoencoder is used in the same way as explained for the pre-

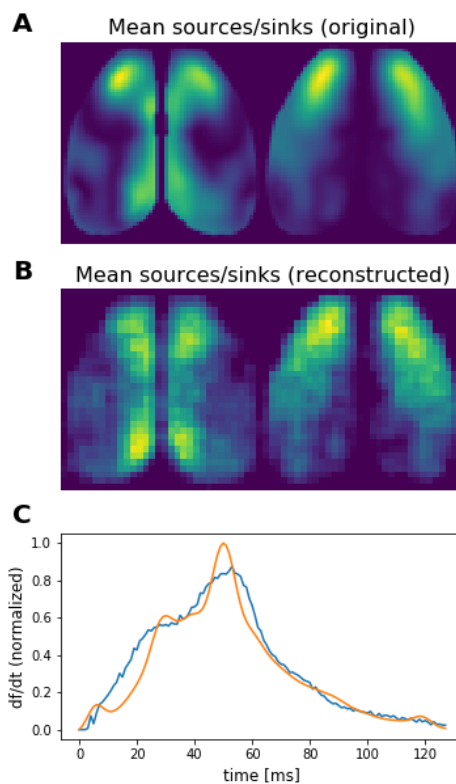


Figure 4.10: Examples for reconstructions of the mixed input model. Panel A: The distribution of sources (left) and sinks (right). Panel B: The reconstructions of the image shown in A. Panel C: The respective df/f signal and the reconstructed signal.

vious one. However it is trained on more features that arguably make up the most important characteristics of neocortical slow waves: The shape of the df/f signal alongside the duration and amplitude, the ratio between flow in different directions as well as the distribution of sources and the distribution

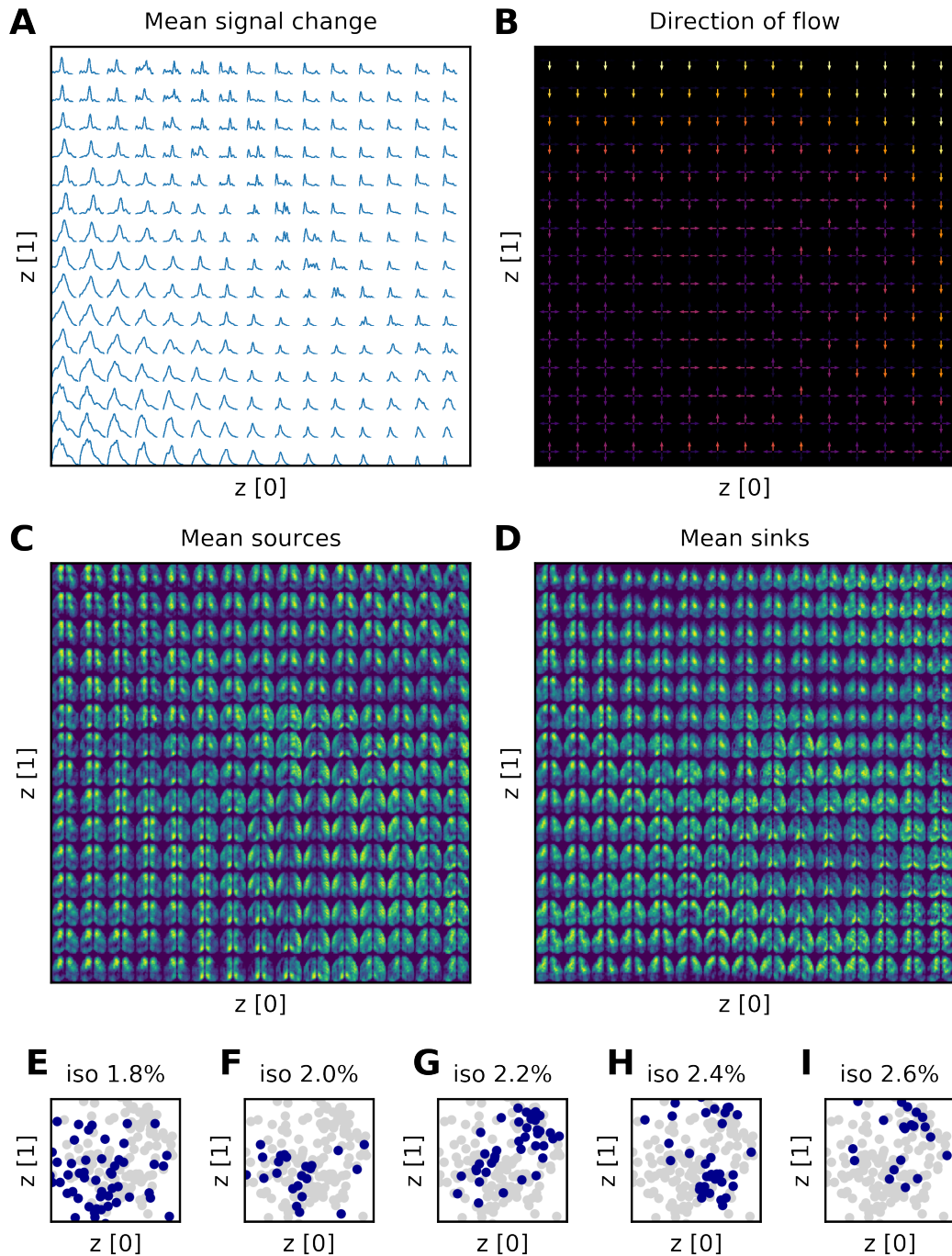
of sinks. Hence latent slow wave space allows for a more complete distinction of neocortical slow waves that most importantluy includes the distribution of focal areas of recurrent activity. The performance of the reconstructions is indicated by Figure 4.10. Although only a two dimensional latent space was used an acceptable reconstruction was achieved for all included features.

The arrangement of slow wave shapes in the latent space of the second Autoencoder differs from the first one. Here large amplitude waves with multiple peaks are mapped to the lower left corner. Large single peak waves correspond to an area between the center and the lower right corner. Small waves that can include a second peak rely above the diagonal in the upper right area. The distibution of sources reveals that the shape of neocortical slow waves is related to focal areas of recurrent activity. Sources in frontal areas are present for small waves that exist mainly during very deep anaesthesia. This type of small waves is charachterized by downwards flow.

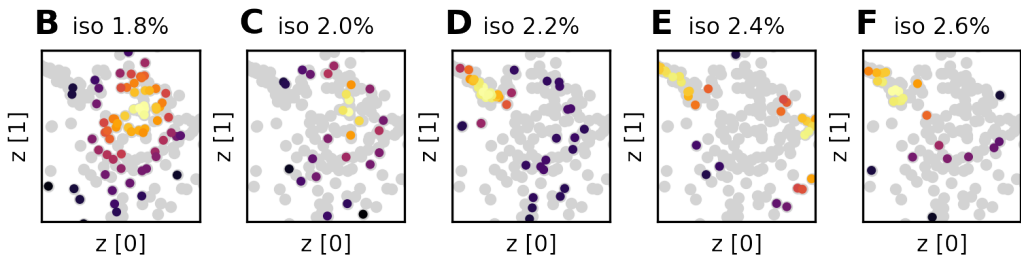
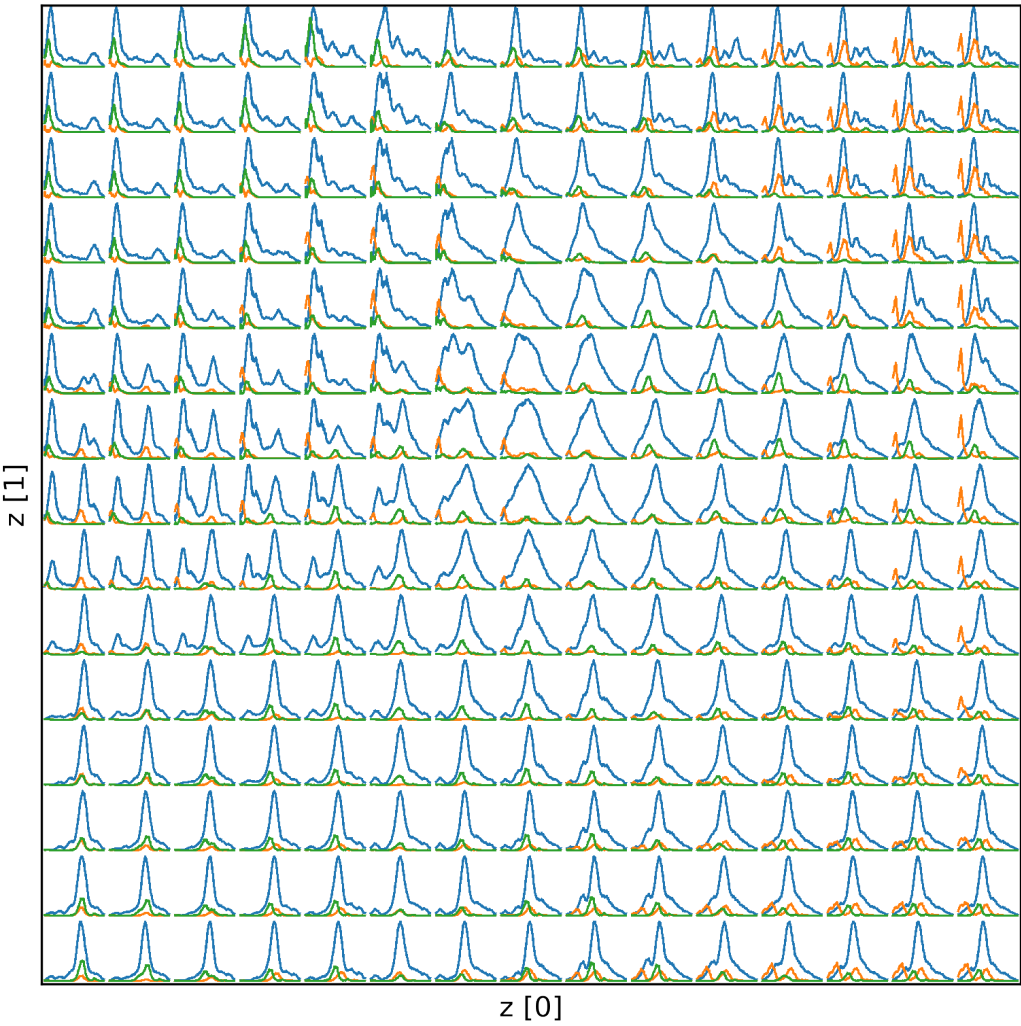
The manifold of sources and sinks provides further information regarding the nature of larger waves. Neocortical slow waves that are mapped to a region to the lower right of the center have sources in areas of the brain that arguably relate to the barrel fields. In contrast, large waves that potentially include multiple peaks have sources either in frontal areas or in a medial band that includes the RSD. Especially for the latter kind of events sinks reside in areas different from the sources and upwards flow dominates. However there are areas as well where the horizontal flow is strong. Visual inspection of the vector field animations shows that this kind of waves includes upwards flow that is strongest in medial portions in early stages of the events while medial lateral flow occurs mainly in frontal areas in later periods. Large neocortical slow waves can exist in the form of medial axis events with bottom up flow and as frontal events that sometimes exhibit pronounced downwards flow.

The latent space mappings described above illustrate a complex topology of neocortical slow waves. However, a third Autoencoder was used to analyse the exact temporal dynamics of upwards and downwards flow in relation to the df/f signal. Here the normalized df/f signal as well as a signal for upwards and downwards flow were used. It shows that a peak in vertical flow occurs during the first major rising phase of neocortical slow waves. Latent space reconstructions reveal events where upwards flow is stronger than

downwards flow and waves where the opposite is the case. In the center left of the reconstruction manifold one may find events with multiple peaks where downwards flow occurs during the first rising phase while upwards flow is stronger during the rise of a second peak.

**Figure 4.11:** Latent slow wave space

The depiction shows the results of for the mixed input model. Note that events with peak-amplitude below 5% signal change and a high correlation with the hemodynamic breathing signal ($r>.3$) were excluded from the analysis. Panel A: Slow wave shape space. The panel shows the reconstructions of the df/f signal for the mixed input model. Duration and amplitude are square root scaled. Panel B: The direction of flow. Arrows indicate the reconstructions for the ratio of flow for each event. Note that upwards flow dominates in the lower center, flow occurs in all directions rather evenly in the middle left portion while downwards flow dominates for events in the upper right area. Panel C and D: The reconstructions of the sources and sinks. Note that differences in the distribution of sources and sinks are most strongly pronounced in the lower central part. Panel E-I: The distribution of samples of different experimental conditions in latent slow wave space. Note that the density of the distribution for overlapping points is color-coded. All samples that do not belong to the respective condition are plotted in grey.

A Signal change, upwards flow and downwards flow

Figure 4.12: Latent slow wave flow space

The depiction illustrates the relationship between the signal change of the fluorescence signal (df/f) and periods of upwards and downwards flow. Autoencoder 3 was used to compute the mappings to latent space and decodings using an evenly spaced grid that covers the majority of points. Panel A: A reconstruction manifold where blue lines relate to the df/f signal. Green lines indicate the strength of upwards flow, as measured by the mean Y component per frame, for periods where this measure is positive. Analogously orange relates to downwards flow. Note that the periods where the vertical flow is most pronounced coincide with the rising phase of the df/f signal. For some events several peaks in flow occur that correspond to several oscillations in the df/f signal. Moreover the preferred direction of flow is not necessarily the same during these subsegements. Panel B-F: The distribution of samples of different experimental conditions in latent slow wave flow space. Note that the density of the distribution for overlapping points is color-coded. All samples that do not belong to the respective condition are plotted in grey.

Chapter 5

Discussion

Summarize your key findings In summary the combination of Optical Flow, Helmholtz Decomposition and Autoencoders reveals a complex topology of different types of neocortical slow waves. It has proven to be a viable approach for the suggested event related analysis of neocortical slow waves. As the literature review showed, neocortical slow waves can originate in cortex spontaneously, however, they can not only be assumed to play an important role for memory but interact with other rythms in the brain. Slow waves can be triggered by subcortical stimulation. They typically incorporate only a subset of strongly interconnected neurons in cortex which results in distinct areas of recurrent activity and patterns of flow. Optical Flow and Helmholtz decomposition can help to measure pathways of flow, centers of recurrent activity and help to distinguish different types of events. Although refinements in the preprocessing might be necessary to further reduce potential artifacts due to hemodynamic effects of breathing the approach can be considered a valid method to study neocortical slow waves using widefield floourescence imaging.

In general it shows that the amplitude of events decreases with the dosage of anaesthesia. The flow-component of the vector fields retrieved with the Horn-Schunck method reveal a complex dynamic of events. Different types of slow waves can be distinguished using autoencoders. Large amplitude waves either refer to medial axis events or events that incorporate frontal regions as sources.

Medial axis events typically include RSD and in some cases show decisive upwards flow, especilly in an early stage. In later stages medial lateral flow can dominate and frontal regions act as centers of recurrent activity. As the

mixed input autoencoder shows slow waves with sources close to the medial axis exhibit a trend towards upwards flow in average. However, the strongest flow can also occur in horizontal direction or in all four main directions for many events. This arguably reflects the described spread from medial to lateral or a complex dynamic of flow patterns. Medial axis events typically have a single peak with a steep rise and decline.

The second type of large amplitude waves incorporates frontal to fronto-parietal sources. In some cases downwards flow is strong, typically however, flow in all main directions occurs. Arguably this reflects that this kind of neocortical slow wave The method represents a valid tool to analyze neocortical slow waves.

Low amplitude waves occur at higher levels of isoflurane. One type of low amplitude wave shows a second peak that is correlated with the hemodynamic breathing signal. This potentially indicates that certain neocortical slow waves are synchronized with a breathing signal. It is unclear, however, whether the breathing synchronized peaks reflect a hemodynamic effect or relate to neural oscillations that occur simultaneously. This implies that further research is necessary to study the interaction between neocortical slow waves and the breathing signal. As the effect of breathing coupled slow waves could easily be removed for anaesthesia levels with a better signal to noise ratio it is advisable to employ the proposed approach for named conditions first.

Helmholtz decomposition helps to distinguish focal areas of recurrent activity from global patterns of flow. It can hence be used as an alternative to approaches that detect the movement of wavefronts. Optical flow allows to measure more complex patterns which is especially important for neocortical slow waves with extended up states that exhibit a complex dynamic that is not sufficiently described by moving wavefronts.

The autoencoder with mixed input arguably allows to distinguish events in the most finegrained manner. Variational autoencoders with two dimensional latent layers appear as a good choice especially because the latent space distributions could easily be interpreted using the manifolds of reconstructions that can be computed for points on an evenly spaced grid using the decoder. This allows to reduce the dimensionality of the data and present it in a way that is intuitively understandable by the reader.

The signal to noise ratio at high levels of anaesthesia represents a challenge.

In addition, a difficulty arises from the circumstance that the standard deviation of the detrended hemodynamic signal increases for higher levels of isoflurane. Moreover the GCaMP signal decreases in strength in these conditions. This means that the experimental conditions are systematically confounded with an error signal. As discussed is unclear what low amplitude oscillations that correlate with breathing relate to. Potentially, additional refinements in the preprocessing might be necessary to further reduce potential artifacts due to hemodynamic effects. To avoid potential effects of spatially nonuniform activity the possibility to compute the contrast to a downstate image for each event should also be assessed. Named problems limits the interpretability of the results achieved for high levels of anaesthesia. Nonetheless, the suggested approach represents a valid method to study slow waves: An event related analysis of neocortical slow waves and the use of variational autoencoders on features retrieved with Optical Flow and Helmholtz decomposition helps to distinguish different events.

Optical Flow, Helmholtz Decompositon and autoencoders can be used to characterize slow waves. This bears multiple potentials for the analysis of neocortical slow waves that occur during sleep but also under anaesthesia. If sleep slow waves foster memory consolidation one may hypothesize that different types of events exist during sleep that reflect the interaction between hippocampal sharp waves and neocortical slow waves. As widefield flourescence microscopy is challanged by the hemodynamic autoflourescence it is advisable to select stages of anaesthesia where neocortical slow wave occcur with a good signal to noise ratio and to employ methodological triangulation. The use of flourescence microscopy in combination with electrophysiological recordings has previously been shown to help in the interpretation of the results. In future Optical Flow Helmholtz Decomposition and Autoencoders could potentially be used to characterize neocortical slow waves and put their properties into perspective with animal behavior or leaning related signals in hippocampus.

Bibliography

- Akert, K (1965). "The anatomical substrate of sleep". In: *Progress in brain research*. Vol. 18. Elsevier, pp. 9–19.
- Akert, Konrad, WP Koella, and R Hess Jr (1951). "Sleep produced by electrical stimulation of the thalamus". In: *American Journal of Physiology-Legacy Content* 168.1, pp. 260–267.
- Akimoto, Haruo et al. (1956). "On the sleep induced through electrical stimulation on dog thalamus". In: *Psychiatry and Clinical Neurosciences* 10.2, pp. 117–146.
- Alex, Varghese et al. (2017). "Semisupervised learning using denoising autoencoders for brain lesion detection and segmentation". In: *Journal of Medical Imaging* 4.4, p. 041311.
- Anwar, Saeed et al. (2020). "Image colorization: A survey and dataset". In: *arXiv preprint arXiv:2008.10774*.
- Arganda-Carreras, Ignacio and David Legland (2016). *Distance Transform Watershed*. URL: https://imagej.net/Distance_Transform_Watershed (visited on 01/01/2021).
- Aulinas, Anna (2019). "Physiology of the Pineal Gland and Melatonin". In: *Endotext [Internet]*. MDText. com, Inc.
- Aussel, Amélie et al. (2018). "A detailed anatomical and mathematical model of the hippocampal formation for the generation of sharp-wave ripples and theta-nested gamma oscillations". In: *Journal of computational neuroscience* 45.3, pp. 207–221.
- Behrens, Christoph J et al. (2005). "Induction of sharp wave–ripple complexes in vitro and reorganization of hippocampal networks". In: *Nature neuroscience* 8.11, pp. 1560–1567.
- Berger, Hans (1929). "Über das elektroenkephalogramm des menschen". In: *Archiv für psychiatrie und nervenkrankheiten* 87.1, pp. 527–570.
- Bernardi, Giulio et al. (2018). "Local and widespread slow waves in stable NREM sleep: evidence for distinct regulation mechanisms". In: *Frontiers in human neuroscience* 12, p. 248.
- Bhatia, Harsh, Valerio Pascucci, and Peer-Timo Bremer (2014). "The natural Helmholtz-Hodge decomposition for open-boundary flow analysis". In: *IEEE transactions on visualization and computer graphics* 20.11, pp. 1566–1578.
- Bhatia, Harsh et al. (2012). "The Helmholtz-Hodge decomposition—a survey". In: *IEEE Transactions on visualization and computer graphics* 19.8, pp. 1386–1404.

- Biotechnology Information, National Center for (2021). *PubChem Compound Summary for CID 3763*. URL: <https://pubchem.ncbi.nlm.nih.gov/compound/Isoflurane> (visited on 01/01/2021).
- Brown, Ritchie E et al. (2012). "Control of sleep and wakefulness". In: *Physiological reviews*.
- Buljubasic, Nediljka et al. (1992). "Effects of halothane and isoflurane on calcium and potassium channel currents in canine coronary arterial cells". In: *Anesthesiology: The Journal of the American Society of Anesthesiologists* 76.6, pp. 990–998.
- Buzsáki, György (1996). "The hippocampo-neocortical dialogue". In: *Cerebral cortex* 6.2, pp. 81–92.
- CEDMAV (2020). *The natural Helmholtz-Hodge Decomposition*. URL: <http://cedmav.org/research/topology/71 - the - natural - helmholtz - hodge - decomposition> (visited on 01/01/2021).
- Celotto, Marco et al. (2020). "Analysis and model of cortical slow waves acquired with optical techniques". In: *Methods and Protocols* 3.1, p. 14.
- Choi, Tae-Yong et al. (2014). "Melatonin inhibits voltage-sensitive Ca²⁺ channel-mediated neurotransmitter release". In: *Brain research* 1557, pp. 34–42.
- Coggan, David D, Daniel H Baker, and Timothy J Andrews (2019). "Selectivity for mid-level properties of faces and places in the fusiform face area and parahippocampal place area". In: *European Journal of Neuroscience* 49.12, pp. 1587–1596.
- De Berardis, Domenico et al. (2011). "The melatonergic system: Effects on sleep and implications for the treatment of psychiatric disorders". In: *ChronoPhysiology and Therapy* 1, pp. 59–67.
- Devor, Anna et al. (2012). "Frontiers in optical imaging of cerebral blood flow and metabolism". In: *Journal of Cerebral Blood Flow & Metabolism* 32.7, pp. 1259–1276.
- Dossi, R Curró, A Nunez, and M Steriade (1992). "Electrophysiology of a slow (0.5-4 Hz) intrinsic oscillation of cat thalamocortical neurones in vivo." In: *The Journal of Physiology* 447.1, pp. 215–234.
- Du, Getao et al. (2020). "Medical image segmentation based on u-net: A review". In: *Journal of Imaging Science and Technology* 64.2, pp. 20508–1.
- Eger, Edmond I (1981). "Isoflurane: A Review". In: *Anesthesiology: The Journal of the American Society of Anesthesiologists* 55.5, pp. 559–576.
- Felleman, Daniel J and David C Van Essen (1991). "Distributed hierarchical processing in the primate cerebral cortex." In: *Cerebral cortex (New York, NY: 1991)* 1.1, pp. 1–47.
- Furrer, Melanie et al. (2019). "Sleep EEG slow-wave activity in medicated and unmedicated children and adolescents with attention-deficit/hyperactivity disorder". In: *Translational psychiatry* 9.1, pp. 1–8.
- Gămănuț, Răzvan et al. (2017). "The mouse cortical interareal network reveals well defined connectivity profiles and an ultra dense cortical graph". In: *bioRxiv*, p. 156976.
- Golowasch, Jorge and Farzan Nadim (2014). "Membrane Capacitance". In: *Encyclopedia of Computational Neuroscience*. Ed. by Dieter Jaeger and Ranu Jung. Springer.

- ISBN: 978-1-4614-7320-6. URL: <http://dblp.uni-trier.de/db/reference/cn/cn2014.html#GolowaschN14>.
- Gould, TJ et al. (2002). "Effects of hippocampal lesions on patterned motor learning in the rat". In: *Brain research bulletin* 58.6, pp. 581–586.
- Graham, Bruce P, Vassilis Cutsuridis, and Russell Hunter (2010). "Associative memory models of hippocampal areas CA1 and CA3". In: *Hippocampal microcircuits*. Springer, pp. 459–494.
- Groen, Thomas van and J Michael Wyss (1992). "Connections of the retrosplenial dysgranular cortex in the rat". In: *Journal of Comparative Neurology* 315.2, pp. 200–216.
- Han, Kuan et al. (2019). "Variational autoencoder: An unsupervised model for encoding and decoding fMRI activity in visual cortex". In: *NeuroImage* 198, pp. 125–136.
- Horn, Berthold KP and Brian G Schunck (1981). "Determining optical flow". In: *Artificial intelligence* 17.1-3, pp. 185–203.
- Hur, Junhwa and Stefan Roth (2020). "Optical Flow Estimation in the Deep Learning Age". In: *Modelling Human Motion*. Springer, pp. 119–140.
- Institute, Max Planck (2020). *MPI Sintel Dataset: Results and rankings*. URL: <http://sintel.is.tue.mpg.de/quant> (visited on 01/01/2021).
- Jenkins, Andrew, Nicholas P Franks, and William R Lieb (1999). "Effects of Temperature and Volatile Anesthetics on GABAAR Receptors". In: *Anesthesiology: The Journal of the American Society of Anesthesiologists* 90.2, pp. 484–491.
- Jercog, Daniel et al. (2017). "UP-DOWN cortical dynamics reflect state transitions in a bistable network". In: *Elife* 6, e22425.
- Ji, Daoyun and Matthew A Wilson (2007). "Coordinated memory replay in the visual cortex and hippocampus during sleep". In: *Nature neuroscience* 10.1, pp. 100–107.
- Kawamura, Hiroshi and Edward F Domino (1968). "Hippocampal slow ("arousal") wave activation in the rostral midbrain transected cat". In: *Electroencephalography and clinical neurophysiology* 25.5, pp. 471–480.
- Kim, Minkyung and Hyun-joon Shin (2019). "Development of all-optical imaging system for studying cerebral blood flow regulation using optogenetics". In: *European Conference on Biomedical Optics*. Optical Society of America, 11076_76.
- Koella, WP (1984). "The organization and regulation of sleep". In: *Experientia* 40.4, pp. 309–338.
- Kostowski, W et al. (1969). "Electrical stimulation of midbrain raphe: biochemical, behavioral and bioelectrical effects". In: *European Journal of Pharmacology* 7.2, pp. 170–175.
- Kramer, Mark A (1991). "Nonlinear principal component analysis using autoassociative neural networks". In: *AIChE journal* 37.2, pp. 233–243.
- Kubin, Leszek (2019). "Interactions Between Sleep and Breathing". In: *Handbook of Behavioral Neuroscience*. Vol. 30. Elsevier, pp. 205–221.

- Kumar, Sandeep, Rohit Raja, and Archana Gandham (2020). "Tracking an Object Using Traditional MS (Mean Shift) and CBWH MS (Mean Shift) Algorithm with Kalman Filter". In: *Applications of Machine Learning*. Springer, pp. 47–65.
- Lee, Jennifer A et al. (2014). "In vivo spectral and fluorescence microscopy comparison of microvascular function after treatment with OXi4503, Sunitinib and their combination in Caki-2 tumors". In: *Biomedical Optics Express* 5.6, pp. 1965–1979.
- Lee, Jungryun, Daesoo Kim, and Hee-Sup Shin (2004). "Lack of delta waves and sleep disturbances during non-rapid eye movement sleep in mice lacking α 1G-subunit of T-type calcium channels". In: *Proceedings of the National Academy of Sciences* 101.52, pp. 18195–18199.
- Lefèvre, Julien et al. (2009). "Identification of growth seeds in the neonate brain through surfacic Helmholtz decomposition". In: *International Conference on Information Processing in Medical Imaging*. Springer, pp. 252–263.
- Lin, Chen-Hsuan, Chen Kong, and Simon Lucey (2018). "Learning efficient point cloud generation for dense 3d object reconstruction". In: *proceedings of the AAAI Conference on Artificial Intelligence*. Vol. 32. 1.
- Lucas, Bruce D, Takeo Kanade, et al. (1981). "An iterative image registration technique with an application to stereo vision". In: Vancouver, British Columbia.
- Lüthi, Anita (2014). "Sleep spindles: where they come from, what they do". In: *The Neuroscientist* 20.3, pp. 243–256.
- Maingret, Nicolas et al. (2016). "Hippocampo-cortical coupling mediates memory consolidation during sleep". In: *Nature neuroscience* 19.7, pp. 959–964.
- Mallick, Pradeep Kumar et al. (2019). "Brain MRI image classification for cancer detection using deep wavelet autoencoder-based deep neural network". In: *IEEE Access* 7, pp. 46278–46287.
- Milczarek, Michal M, Seralynne D Vann, and Frank Sengpiel (2018). "Spatial memory engram in the mouse retrosplenial cortex". In: *Current Biology* 28.12, pp. 1975–1980.
- Miller, Amanda L, Danny Theodore, and Jason Widrich (2020). "Inhalational anesthetic". In: *StatPearls [Internet]*. StatPearls Publishing.
- Moghadam, Hadi et al. (2019). "A Comparative Study of Cell Specific Effects of Systemic and Volatile Anesthetics on Identified Motor Neurons and Interneurons of Lymnaea stagnalis (L.), Both in the Isolated Brain and in Single Cell Culture". In: *Frontiers in Physiology* 10, p. 583.
- Montagna, Pasquale (2005). "Fatal familial insomnia: a model disease in sleep physiopathology". In: *Sleep medicine reviews* 9.5, pp. 339–353.
- Murphy, Michael et al. (2009). "Source modeling sleep slow waves". In: *Proceedings of the National Academy of Sciences* 106.5, pp. 1608–1613.
- Neske, Garrett T (2016). "The slow oscillation in cortical and thalamic networks: mechanisms and functions". In: *Frontiers in neural circuits* 9, p. 88.
- Nghiem, Trang-Anh E et al. (2018). "Two types of slow waves in anesthetized and sleeping brains". In: *bioRxiv*, p. 430405.

- Niethard, Niels et al. (2018). "Cortical circuit activity underlying sleep slow oscillations and spindles". In: *Proceedings of the National Academy of Sciences* 115.39, E9220–E9229.
- PapersWithCode (2021a). *Denoising Autoencoders*. URL: <https://paperswithcode.com/method/denoising-autoencoder> (visited on 02/01/2021).
- (2021b). *Sparse Autoencoders*. URL: <https://paperswithcode.com/method/sparse-autoencoder> (visited on 02/01/2021).
- Plaut, Elad (2018). "From principal subspaces to principal components with linear autoencoders". In: *arXiv preprint arXiv:1804.10253*.
- Qazzaz, Munir M and William Winlow (2017). "Modulation of the passive membrane properties of a pair of strongly electrically coupled neurons by anaesthetics". In: *EC Neurol* 6, pp. 187–200.
- Shi, Shoi, Arthur Millius, and Hiroki R Ueda (2019). "Genes and Ion Channels in the Circadian and Homeostatic Regulation of Sleep". In: *Handbook of Behavioral Neuroscience*. Vol. 30. Elsevier, pp. 181–193.
- Shi, Shoi and Hiroki R Ueda (2018). "Ca₂₊-Dependent Hyperpolarization Pathways in Sleep Homeostasis and Mental Disorders". In: *Bioessays* 40.1, p. 1700105.
- Sital, Cheryl et al. (2020). "3D medical image segmentation with labeled and unlabeled data using autoencoders at the example of liver segmentation in CT images". In: *arXiv preprint arXiv:2003.07923*.
- Spiers, Hugo J, Eleanor A Maguire, and Neil Burgess (2001). "Hippocampal amnesia". In: *Neurocase* 7.5, pp. 357–382.
- Steriade, M and M Deschenes (1984). "The thalamus as a neuronal oscillator". In: *Brain Research Reviews* 8.1, pp. 1–63.
- Steriade, Mircea, Angel Nunez, and Florin Amzica (1993). "A novel slow (< 1 Hz) oscillation of neocortical neurons in vivo: depolarizing and hyperpolarizing components". In: *Journal of neuroscience* 13.8, pp. 3252–3265.
- Strang, Gilbert and Edwin Herman (2018). "Divergence and Curl". In: *Hippocampal microcircuits*. Vol. 1. OpenStax, pp. 459–494.
- Stroh, Albrecht et al. (2013). "Making waves: initiation and propagation of corticothalamic Ca₂₊ waves in vivo". In: *Neuron* 77.6, pp. 1136–1150.
- Tort, Adriano BL et al. (2018). "Parallel detection of theta and respiration-coupled oscillations throughout the mouse brain". In: *Scientific reports* 8.1, pp. 1–14.
- Townsend, Rory G and Pulin Gong (2018). "Detection and analysis of spatiotemporal patterns in brain activity". In: *PLoS computational biology* 14.12, e1006643.
- Vertes, Robert P, Stephanie B Linley, and Walter B Hoover (2015). "Limbic circuitry of the midline thalamus". In: *Neuroscience & Biobehavioral Reviews* 54, pp. 89–107.
- Villablanca, Jaime R (2004). "Counterpointing the functional role of the forebrain and of the brainstem in the control of the sleep–waking system". In: *Journal of sleep research* 13.3, pp. 179–208.

- Wu, Jian-Young, Xiaoying Huang, and Chuan Zhang (2008). "Propagating waves of activity in the neocortex: what they are, what they do". In: *The Neuroscientist* 14.5, pp. 487–502.
- Zhang, Jia-Tao, Ah-Chung Tsoi, and Sio-Long Lo (2014). "Scale invariant feature transform flow trajectory approach with applications to human action recognition". In: *2014 International Joint Conference on Neural Networks (IJCNN)*. IEEE, pp. 1197–1204.